3.3 Adsorption on Ru (0001)

The adsorption of atoms and molecules on surfaces has a decisive role in the sequence of catalytic reactions since almost all of them have been confirmed to proceed via the Langmuir-Hinshelwood mechanism, where the reactants adsorb to the surface prior to the reaction, as opposed to the Eley-Rideal mechanism, where at least one of the reactants does not attach to the surface before reacting but rather stays in contact only with the other adsorbates during the reaction. Of the different ways of adsorption we shall concentrate only on the chemisorption; in this case the adsorbates form chemical bonds with the substrate and are thus strongly bound. Then the site for adsorption is a one with a high symmetry like those shown above for the hcp (0001) surface. The depth of the adsorption well, or the adsorption energy, depends on the adsorption site and thus the lateral coordinates of the adsorbate map – if the vertical coordinate is optimised at each lateral position and we simply forget the small influence of the substrate atoms – a two dimensional potential energy surface whose changes yield the corrugation *i. e.* the dependence of the energy on the lateral position. In a case of large corrugation there usually remain only one or few minima for adsorption, or if the potential energy surface is rather flat the diffusion can occur at lower temperatures and thus the adsorbate can temporarily change the adsorption site.

When the atoms or molecules are adsorbed on the surface they do not only interact with the substrate but – at the latest when the coverage approaches a full mono-layer *i. e.* the atom density is the same as of the substrate – mutually. This can occur directly either due to a direct over-lap of the electronic states of the adsorbates, electro-statically through the space above the surface between the adsorbates or indirectly by a change of the substrate and subsequently at the other adsorbate *i. e.* via substrate. The identification of the governing mechanism is in general difficult since *e. g.* the adsorption initially changes the geometry and thus the electronic structure of the surface although the adsorbate-adsorbate interaction would have a direct mechanism. If the adsorbate-adsorbate interaction is repulsive the adsorbates try to avoid each other, and if the repulsion is larger than the corrugation of the potential energy surface some of the adsorbates may enter an adsorption site different from the one preferred in the case of a single adsorbate, the adsorbates can form small domains inside which the adsorption site is the original one but at the boundaries of the domains the regular pattern is not continuous, the adsorbates can cause a lowering of the symmetry or the adsorbate layer arranges itself into an incommensurate, yet highly symmetric over-layer but with a different adsorbate-adsorbate distance and thus registry than that of the substrate; an example of the latter, a compressed and rotated structure for the carbon monoxide adsorbed at the Ru (0001), will be shown below. Similar structures can form if the adsorbate-adsorbate interaction is attractive and stronger than the corrugation, at low coverages clustering of the adsorbates takes place if the adsorbates only can diffuse along the surface or are deposited to the surface within the range of their attractive interaction. However we shall below concentrate on ordered, commensurate over-layers but changing the coverage we can observe trends in the adsorbate-adsorbate interaction. The adsorbates which we have chosen to be presented here are characteristic ad-species in catalytic reactions and constitute a precursor to the studies on the co-adsorption in the following Section.

We have investigated the adsorption of the most effective alkali metals cesium. The large size of a cesium atom or ion and the long range of the electro-static interaction between the adsorbates make a full mono-layer already energetically inferior with respect to the formation of a second adsorbate layer *i. e.* a bi-layer system. We wanted to perform calculations of the single adsorbate layer over

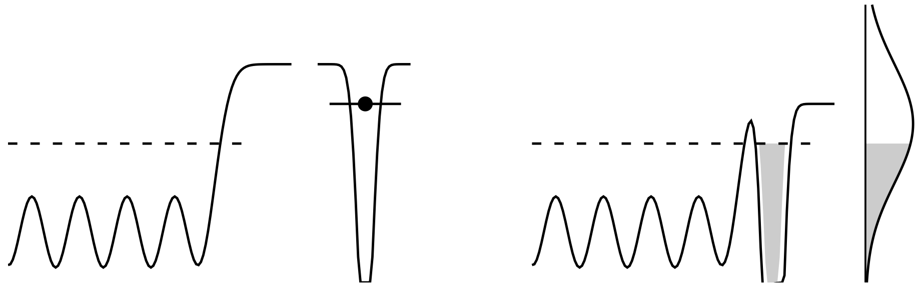

Figure 3.14: A model for the adsorption of an alkali metal due to the Langmuir-Gurney model. On the left the alkali atom is far apart from the surface and its outer-most *s* orbital is occupied with one electron. Upon the adsorption the alkali its *s* level broadens due to hybridisation with the metal bands; the corresponding density of states on the alkali ion is shown at the right, and only the part below the Fermi level – dashed line – is occupied

a wide range of adsorbate-adsorbate distance, or coverages, and we shall make a short summary of the other systems of adsorption of an alkali metal we have studied. The carbon monoxide is an important molecule in several catalytic reactions and is the most studied molecular adsorbate in the literature of the surface science. Furthermore we shortly studied the adsorption of the atomic oxygen, an inhibitor to many reactions but also a reactant in some reactions.

3.3.1 Adsorption of cesium

The famous question concerning the adsorption of alkali atoms on a surface is whether the binding mechanism is ionic or covalent. We do not want to elaborate on this issue since according to our opinion it depends on the definition of ionic or covalent bonding and is thus not uniquely defined. However, according to the current understanding the picture which emerges from the vast number of studies devoted to the adsorption of alkalis is that the alkali denotes partially its outer-most, weakly bound *ns* electron to the hybrids formed with the substrate electrons causing the nucleus to be partially positively charged and a simultaneous reduction in the work function. The adsorption of alkali metal atoms on surfaces is an issue in itself but we shall limit ourselves mainly to the basic properties necessary to discuss the co-adsorption later.

The model traditionally used to describe the adsorption of alkali metals originates from the work of Langmuir and Gurney in the 1920's and 1940's – for a review please see *e. g.* Diehl and McGrath (1997). There the alkali has partially donated its loosely bound valence electron as discussed above, leaving the ion partially positive. This model has been widely used in the literature in the past but was challenged by the early density functional calculations of Wimmer *et al* (1983) who concluded that instead of ionisation the alkali polarises by forming hybrids of its loosely bound electron with the surface electrons. The Langmuir-Gurney model states that the density of electronic states of the alkali atom approaching the surface is like shown in the Figure 3.14: when far from the surface the valence electron of the alkali atom resides fully around the alkali atom. When approaching the surface the electronic level broadens and is only partially occupied.

The electron is distributed to the hybrids with the surface electrons and the positive extra charge forms an image charge at the surface like schematically shown in the Figure 3.15 for a free-electron like surface. The interaction energy is

$$E_{\mathrm{image}} \propto -\mu^2/l^3 \ , \tag{3.1}$$

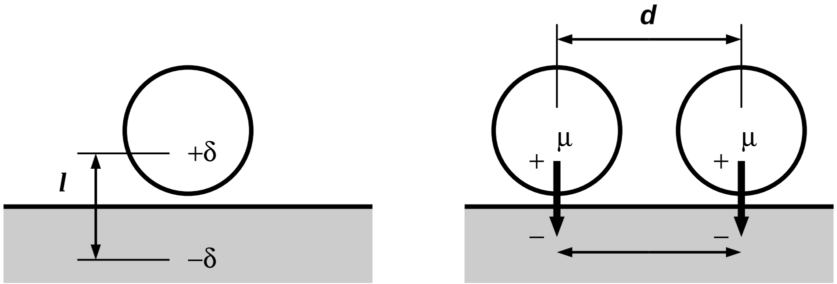

Figure 3.15: A schematic illustration of the electro-static interactions of electro-positive atoms on a metal surface, described here as a continuous electron gas. The attractive interaction between the charge on the ion and its image charge is on the left and the repulsive dipole-dipole interaction on the right

where l is the vertical distance between the charge and its image charge and μ is the dipole moment which can be approximated as two point charges with charge δ and distance l, thus $\mu = l\delta$. Please note that both l and δ would depend on the coverage.

The alkali atoms reveals a positive charge above the surface. Thus when the coverage increases the adsorbate-adsorbate interaction increases and is repulsive; the alkalis repel therefore each other on the surfaces of transition metals. The dipole-dipole interaction is

$$E_{\mathrm{dipole}} \propto +\mu^2/d^3 \ , \tag{3.2}$$

where d is the lateral distance between the dipoles as shown in the Figure 3.15; the adsorbate-adsorbate interaction is thus lateral whereas the image interaction is vertical. From the Equations 3.1 and 3.2 it is obvious that in the high coverages the alkali-alkali repulsion overcomes the attraction of the charge with its image charge. Furthermore the direct Hartree repulsion between the adsorbates increases at smaller distances because the partially screened positive charges start to interact.

When the coverage increases up to about 1/4 the work function begins to increase, approaching the value of the clean alkali metal. In the model of Langmuir and Gurney this is due to metallisation, *i. e.* formation of electronic bands close to the Fermi energy by the over-lapping states due to the adsorbates and thus giving rise to conductivity, in the alkali over-layer because the partially ionised alkali metal atoms start to interact also with each other and in order to reduce the electro-static dipole-dipole repulsion the alkali atoms reduce their ionicity, thereby decreasing the surface dipole and thus the change in the work function. Evidence for the metallisation came from the meta-stable de-excitation spectroscopy – *MDS* – (Woratschek *et al*, 1985) measurements (Fichtner-Endruschat *et al*, 1998), where the enhanced conversion of excited helium atoms from the triplet to singlet states was interpreted as a metallic layer; the earlier results (Böttcher *et al*, 1994; Woratschek *et al*, 1985) from lithium and sodium on Ru (0001) and cesium on Cu (110) have shown the meta-stable de-excitation spectroscopy to be well suited for detecting the state of metallisation. Jacobi *et al* (1994) suggested that the degree of localisation of the valence electrons could be used as an indicator of the metallisation. The vibrational frequency and intensity of the vertical ν(Cs-Ru) mode measured by He and Jacobi (1996) is shown in the Figure 3.16: First the frequency increases with coverage, by a magnitude which has not been explained so far, and then decreases. After the coverage 0.23 the vibrational loss is no longer detectable and an electronic excitation, plasmon, occurs. This was interpreted as full screening of the dynamical surface dipole induced by the cesium due to the

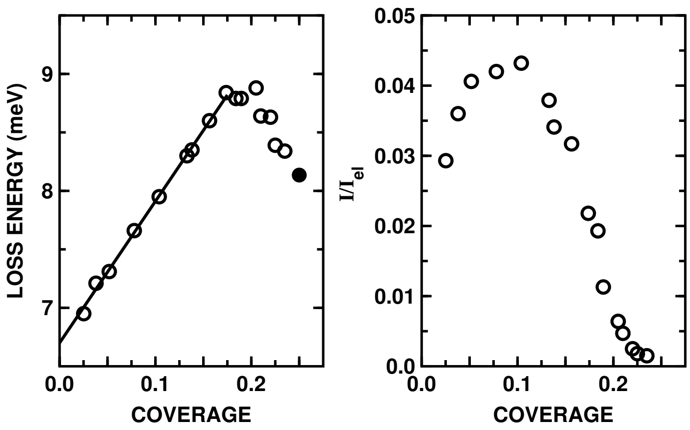

Figure 3.16: The vibrational frequency and intensity of cesium on Ru (0001) measured with the high-resolution electron energy loss spectroscopy by He and Jacobi (1996). The frequency with the filled circle is from our density functional calculations

metallisation of the over-layer.

As an example of the dipole interactions we show the evaluation of the energy components done by Over *et al* (1995a) based on the measurement of the work function by Hrbek (1985). From the work function one obtains the dipole moment by the Helmholtz equation and using a constant distance l=3.0 Å between the cesium ion and its image one obtains the total energy which is first highly attractive and at coverages > 0.2 repulsive relative to adsorbates at infinite separation. Above the coverage ≈ 0.33 the repulsion weakens slightly, due to the reducing dipole moment. However, the higher coverages are not stable due to the adsorbate-adsorbate repulsion because of the increase of the kinetic energy when the outer-most *s* orbitals start to overlap, and thus the Pauli repulsion increases rapidly. The large extent of the 6*s* wave function is evident from the Figure 3.18 which shows the overlap of the atomic orbitals between the closest-neighbour alkali-alkali pair; the 6*s* orbitals have their maxima close to the mid-point between the two atoms, and therefore a large penalty in the kinetic energy, part of which is won back due to the re-hybridisation, has to be paid in order to orthogonalise these orbitals. Part. The Figure 3.19 gives an estimation of the kinetic energy for a hexagonal mono-layer of cesium as a function of the nearest-neighbour distance; the sum grows approximately linearly with coverage. What is still missing from the energy in the Figure 3.19 is the hybridisation between the adsorbate and the substrate, and the electro-static and exchange-correlation adsorbate-adsorbate interactions beyond the dipole-dipole repulsion.

The effective size, describable *e.g.* with the Pauling radius, of the alkali atoms when adsorbed on the Ru (0001) surface shows that the alkali resides rather far from the surface (please see Over *et al*, 1995a) – even the smallest of them, lithium, in the $(\sqrt{3}\times\sqrt{3})$R30° structure has a larger inter-layer distance than ruthenium (Gierer *et al*, 1995). Therefore the distance to the substrate atoms underneath the alkali atom at different adsorption sites does not vary much and also the features of the electron structure smear out. Thus the corrugation of the potential energy surface for the adsorption of an alkali atom is rather small, and especially at large coverages the adsorbate-adsorbate repulsion determines the adsorption site and geometry rather than the adsorbate-substrate interaction. The Figure 3.20 depicts the phase diagram for Cs adsorption on Ru (0001) determined from low energy electron diffraction experiments by Over *et al* (1992b); in addition to the two ordered structures – $(\sqrt{3}\times\sqrt{3})$R30° and (2×2) – there appear rotated structures where the adsorption sites are no longer only the high-symmetry sites. The ring structures indicate a liquid-like structure with

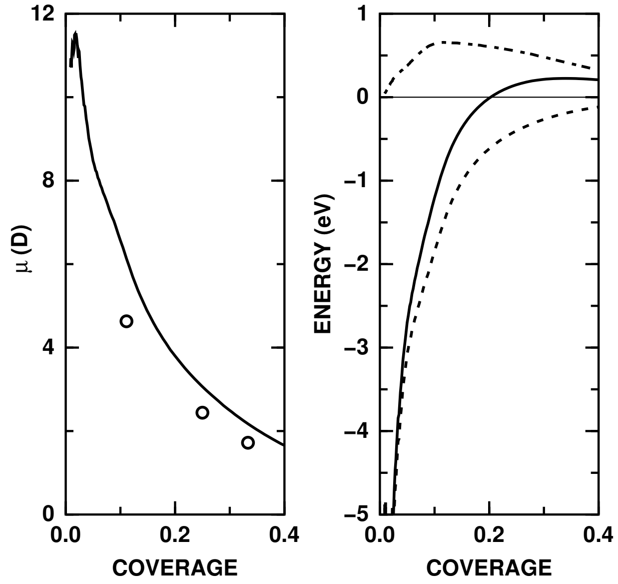

Figure 3.17: *Left*: The dipole moment of cesium adsorbed on the Ru (0001) surface; *Right*: the estimated resulting image force – dashed line – and dipole-dipole – dot-dashed line – energies, and their sum – solid line. The circles are values from our density-functional calculations. After Over *et al* (1995a)

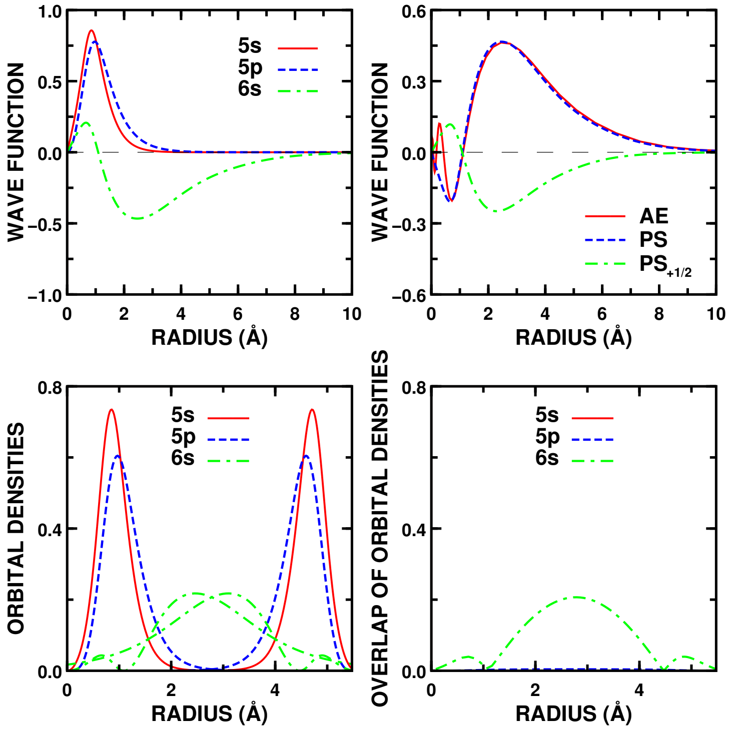

Figure 3.18: The pseudo wave functions of the valence and semi-core orbitals – upper left –, the 6s wave function in the neutral and half-ionised atom – upper right –, the orbitals of nearest-neighbour atoms corresponding to the distance in the (2×2) structure on Ru (0001) – lower left – and the overlap of the orbital densities – lower right, defined as $\sqrt{u_{lm}^2\left(|\mathbf{r}-\mathbf{R}_1|\right) \cdot u_{lm}^2\left(|\mathbf{r}-\mathbf{R}_2|\right)}$. The wave functions are multiplied with the radius so that the integral of the squared wave function over the radius gives one electron. In the ionised case the orbital was scaled with the occupation factor 1/2

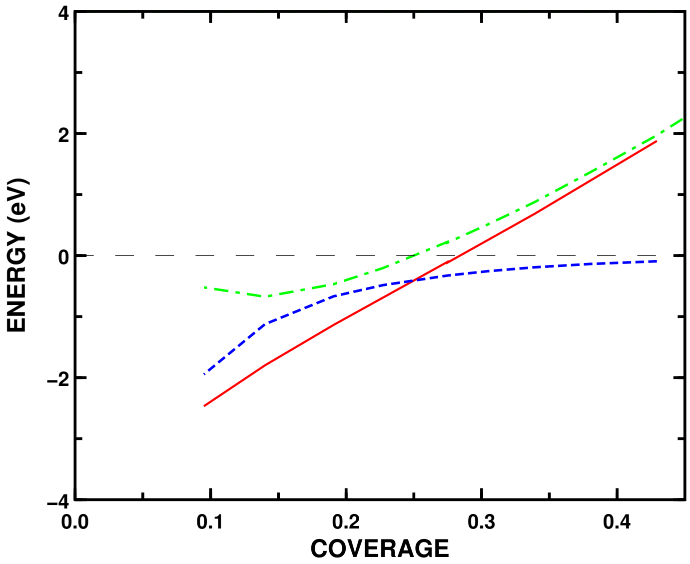

Figure 3.19: The kinetic energy of a free mono-layer of cesium – dot-dashed line –, the dipole-dipole and dipole-image interactions of cesium on Ru (0001) – dashed line – and the sum of them – solid line; the kinetic energy of the free atom has been subtracted, and the absolute position of the vertical axis is arbitrary

a constant mean spacing between the adsorbates and no azimuthal ordering with respect to the substrate.

The weak corrugation of the potential energy surface for the alkali adsorption makes the prediction of the adsorption site difficult, and on the Ru (0001) the adsorption site changes between the $(\sqrt{3} \times \sqrt{3})\mathrm{R}30°$ and (2×2) over-layers for alkali atoms sodium, potassium, rubidium and cesium (Over *et al*, 1995a). For lithium only Doering and Semancik (1986) have reported a (2×2) pattern but it has not been reproduced up to date. In all the $(\sqrt{3} \times \sqrt{3})\mathrm{R}30°$ structures the alkali resides on the three-fold hollow hcp site whereas except for the on-top site of cesium the lighter alkali atoms sit on the other three-fold hollow site – fcc – in the observed (2×2) structures.

We have performed density functional calculations for cesium in the $(\sqrt{3} \times \sqrt{3})\mathrm{R}30°$, (2×2) and (3×3) structures. The main results are summarised in the Table 3.3 and the geometries in the Figure 3.21. Higher coverages with pseudo-morphic ordering are not probable since the next ordered structure with a single adsorption site would contain nearest-neighbour distances of 2.70 Å, while the smallest of the Pauling radii, ionic radius, of cesium is 1.69 Å and thus even the ionic radii would overlap. Thereby no nearest-neighbour pair of cesium is likely to occur and furthermore, as discussed above, at these coverages the cesium atoms are more metallic than ionic and the covalent and metallic radii of cesium are much larger, 2.35 Å and 2.67 Å respectively.

The adsorption energy demonstrates clearly the repulsion between the adsorbates – cf the Figure 3.22, being still large beyond the third-nearest neighbour distance in the (2×2) structure; the magnitude is in good agreement with the heat of adsorption estimated from the simulations of thermal desorption experiments by Payne *et al* (1996). Here it is important to compare the values derived from the experiments with the theoretical desorption energies obtained assuming a "sequential abstraction" as explained in the Section 2.5.2. The calculated values are above the values of Payne *et al* at all the three coverages but this can be a systematic overestimation, namely if the alkalis still interact in the (3×3) structure the first point, at the coverage 1/9, should be lower and this would decrease also the value at the coverage 1/4. The cohesion energy, marked with the arrow

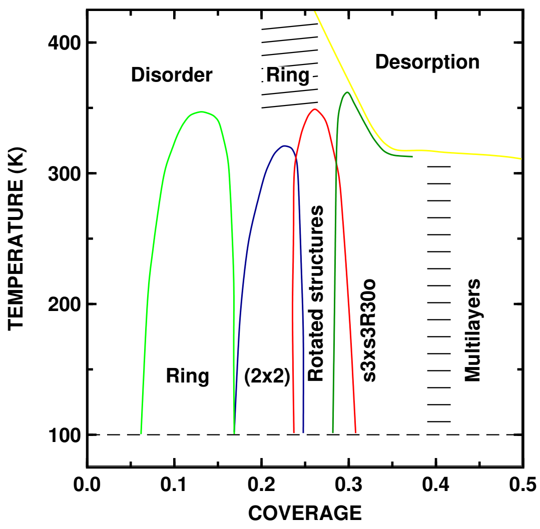

Figure 3.20: Phase diagram for the adsorption of cesium on the Ru (0001) surface as determined from the low energy electron diffraction experiments by Over *et al* (1992b)

Table 3.3: The adsorption energy, the change in work function from the clean surface, the dipole moment, the height of cesium above the nearest ruthenium atom and the cesium-ruthenium distance for cesium adsorbed on Ru (0001). All energies are in electron volts and distances in Ångströms; the dipole moments are in Debyes

Structure	Site	E_{ads} (eV)	$\Delta\phi$ (eV)	μ (D)	Z_{Cs} (Å)	d_{Cs-Ru}
$(\sqrt{3}\times\sqrt{3})R30^\circ$	hcp	1.760	-3.24	1.73	3.08	3.50
	fcc	1.754	-3.22	1.72	3.09	3.51
	on-top	1.674	-3.23	1.72	3.14	3.14
(2×2)	hcp	1.945	-3.48	2.47	3.11	3.52
	fcc	1.945	-3.45	2.45	3.11	3.52
	on-top	1.936	-3.44	2.44	3.16	3.16
(3×3)	hcp	2.275	-2.90	4.63	3.19	3.58
	on-top	2.242	-2.93	4.68	3.22	3.22

Table 3.4: A comparison between the results obtained with two different pseudo potentials for the cesium. The first pseudo potential is used in all the other calculations, and the second one has only smaller core radii at the *s* and *p* channels

Structure	Site	E_{ads}	$\Delta\phi$ (eV)	μ (D)	Z_{Cs} (Å)	d_{Cs-Ru}
1^{st} pseudo potential	hcp	1.945	-3.48	2.47	3.11	3.52
	on-top	1.936	-3.44	2.44	3.16	3.16
2^{nd} pseudo potential	hcp	1.756	-3.46	2.49	3.14	3.54
	on-top	1.756	-3.50	2.46	3.18	3.18

at the right hand side in the Figure 3.22, of bulk cesium from the density functional calculations is slightly smaller than in the results of Payne *et al*. Since the experimental desorption temperature between the first and subsequent cesium layers differs only slightly the adsorption energy at full- and multi-layer coverages must be similar at different coverages of cesium beyond $\Theta_{Cs} \approx 0.25$. Our results of the lower adsorption energy in the (3×3) than in the (2×2) structure does not necessarily imply the formation of an ordered (3×3) structure at coverage of 1/9 even at very low temperatures since the energy difference between the adsorption sites or in different over-layer spacings is close to the thermal energy $k_B T$. Please note further that the change in the work function is linear only up to a distance corresponding to about (5×5) structure – $\theta = 0.04$ – suggesting an interaction between the adsorbates, possibly via the substrate or electro-statically, up to these distances.

The very small difference in the adsorption energy between the different adsorption sites agrees well with the experimental findings of disordering already at low temperature (Over *et al*, 1992b), low frequency for the lateral motion and the large amplitude of displacement (Over *et al*, 1995d) in the low-energy energy diffraction measurement employing the method of split positions. The small differences set very high demands for the accuracy of the calculations, and the adsorption site in the (2×2) structure is erroneous in our results – the on-top site preferred in the experiments is higher in energy than the three-fold hollow sites. The difference from $(\sqrt{3} \times \sqrt{3})R30°$ to (2×2) is, however, correct since the adsorption energy of cesium on the on-top site becomes relatively more attractive than the three-fold hollow sites. Therefore – and considering the magnitude of the energy differences – we do not regard the error as significant. A possible source of error besides the numerical approach and usage of pseudo potentials in our calculations is the negligence of the zero-point and thermal vibrations; to estimate their effect the potential energy surface or at least the lateral and vertical vibrational frequencies should be calculated.

In order to identify the possible sources of error in predicting adsorption site we repeated the calculation of the cesium on the hcp and on-top sites in the (2×2) structure using a different pseudo potential which had smaller core radii for the 5*s* and 5*p* projectors and included the non-linear core-valence exchange correlation scheme explained in the Section 2.3.4. The results are collected in the Table 3.4, and they show very close agreement otherwise but the adsorption energies of the hcp and on-top sites are not practically identical, suggesting the difficulty in the prediction of the adsorption sites might be caused by small but in this case sensitive details of the calculation. A further test *e.g.* on the effect of the **k** sampling should be still performed to exclude an error due to it alone. Also the neglect of spin-orbit coupling and relavistic effects among the valence electrons might be responsible for the small but non-vanishing error.

The long adsorption distance is evident from the geometries shown in the Figure 3.21 and the

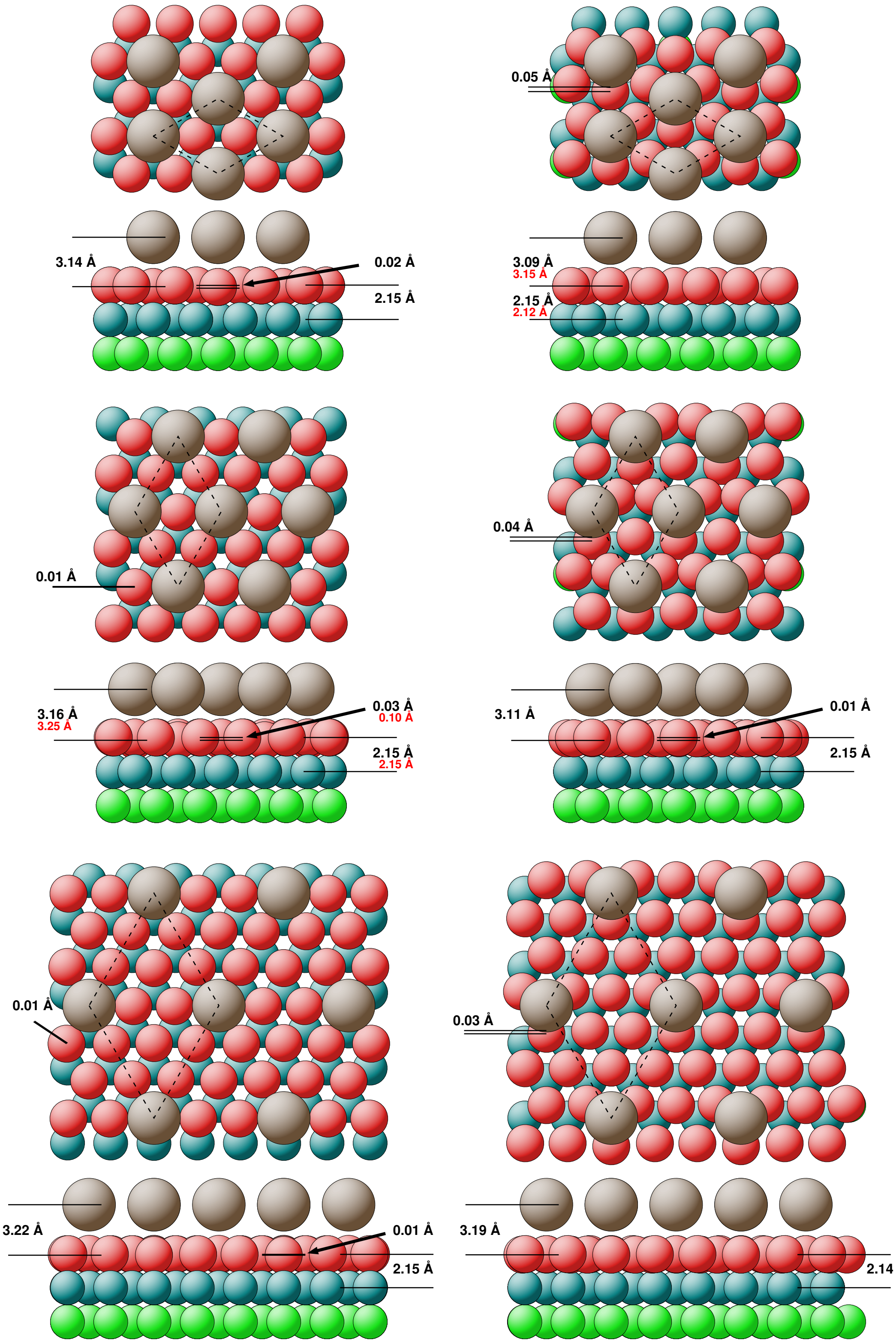

Figure 3.21: The adsorption geometry of cesium on Ru (0001) from our density functional calculations and experiments in the $(\sqrt{3} \times \sqrt{3})R30°$, (2×2) and (3×3) structures; the structures with the cesium atoms adsorbed at the on-top site are on the left and at the hcp site are on the right side. The experimental results from Over *et al* (1992b) are shown with the smaller font

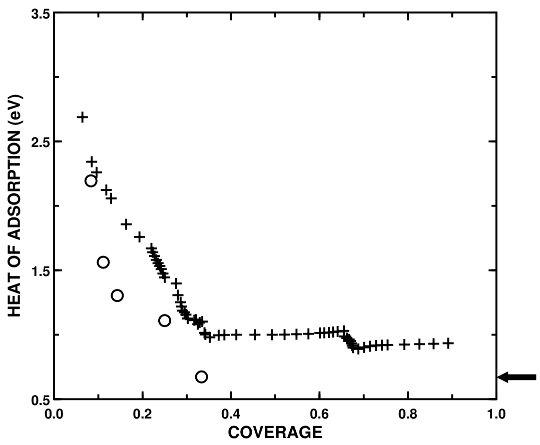

Figure 3.22: The heat of adsorption estimated by Payne *et al* (1996) – crosses – from the simulated thermal desorption curves and the adsorption energy from our density functional calculations – circles; the calculated cohesion energy of bulk cesium is shown with the arrow on the right of the plot

Table 3.3. Our distances agree well in the magnitude with the results from the low energy electron diffraction. Again the exclusion of the zero-point and thermal vibrations can cause an error; their inclusion – especially the vertical one – would prefer a larger distance from the surface since the potential energy rises more steeply towards the surface, and this effect is largest at the on-top site where there is a ruthenium atom beneath the alkali atom. In order to gain insight on the magnitude of this effect we calculated the one-dimensional potential energy surface for the vertical motion of cesium – *i. e.* the surface is kept fixed and neglecting lateral degrees of freedom of cesium are neglected – in the (2×2) cell with the cesium atom at the on-top adsorption site. The potential energy is shown in the Figure 3.23 together with the ten lowest-energy wave packets obtained from the one-dimensional Schrödinger equation for a particle with a mass equal to that of the cesium atom. The frequency obtained from the potential energy surface is included in the Figure 3.16 and is 8.135 meV if evaluated classically, *i. e.* directly from the curvature and 8.168 meV if taken as twice the energy of the lowest-energy solution of the quantum mechanical Schrödinger equation, in very good agreement with the experiments. The large amplitude of the wave packets already prompts to a large amplitude for the vertical movement, but they are almost symmetric and thus the centre of mass of the wave packet, calculated at an kinetic energy $\frac{1}{2}k_B T$ corresponding to a temperature of 100 K where the experiments are usually carried out, shows only an increase in the vertical distance of 5 mÅ.

The atomic distances and heights between the cesium and nearest-neighbour ruthenium atoms show interesting trends: The height of Cs above the ruthenium surface is almost identical at a given coverage between different adsorption sites; thus the Cs-Ru distance is much smaller at the on-top sites, in variance with the expectation from the model of Langmuir and Gurney that the alkali atom would prefer a high-coordinated site in order to bond to as many atoms as possible since in the (2×2) geometry the alkali adsorbs at the on-top site leading to a much smaller and single bond than it would achieve at the three-fold hollow sites. Furthermore the Cs-Ru layer height and distance on a given site decreases with increasing coverage, although the metallic radius of cesium is larger than the ionic radius and thus the metallisation occurring beyond coverage $\approx 1/4$ would require an increase upon increasing coverage. The same trend of apparently decreasing size of the alkali

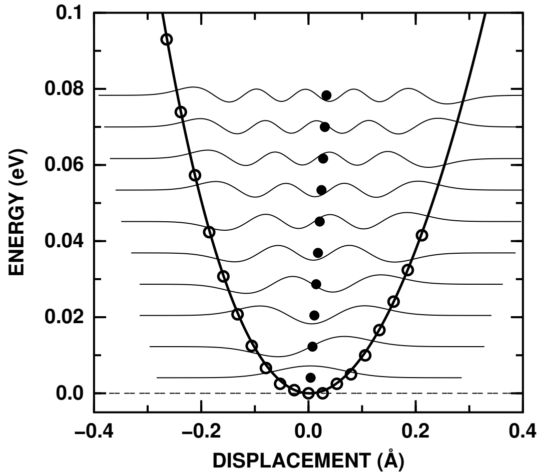

Figure 3.23: The potential energy surface – circles, calculated points by empty spheres and a polynomial fit by the thick line – for the vertical movement of cesium on Ru (0001) from our density functional calculations in the (2 × 2) structures. The ten lowest-energy solutions of the Schrödinger equation and their centres of mass in this potential are also shown

atom with increasing coverage was seen in the experiments of Schuster, Eng and Robinson (1995) using X-ray diffraction for cesium on the Ag (110), from the low energy electron diffraction studies of Kaukasoina *et al* (1997) for potassium, rubidium and cesium on the Ag (111), and by Wedler *et al* (1993) employing diffuse low electron energy diffraction for potassium on the Ni (100) surface.

Over *et al* (1995a) connected the site preference upon adsorption to the buckling of the outermost substrate layer and this way to the bulk modulus of the substrate: in the (2 × 2) structure – and lower coverages – the cesium atom at the on-top site can form a semi-seven-fold adsorption site depicted in the Figure 3.24 by shifting the atom beneath the cesium towards the bulk – *i. e.* buckling – thereby better screening the dipoles from the other cesium atoms; the smaller the bulk modulus of the substrate, the easier it is to achieve the buckling. This effect is no longer efficient in the $(\sqrt{3} \times \sqrt{3})R30°$ structure since the cesium atoms are already too close to each other and the screening by ruthenium atoms would no longer be sufficient, and therefore cesium now adsorbs on the high-coordinated hcp site. The lighter alkalis have a smaller dipole at the surface and are also smaller, and they do not need to adsorb at the on-top site in order to screen their dipoles but are placed at the fcc site in the $(\sqrt{3} \times \sqrt{3})R30°$ structure. However, in our calculations the change in work function for potassium at the hcp site in the $(\sqrt{3} \times \sqrt{3})R30°$ structure is smaller by 0.13 eV than for cesium, thus the dipole moment is only about 4 % smaller for potassium than for cesium. This does not support a large difference between the two different alkalis, again demonstrating the delicate balance between the adsorption at different sites.

Next we come to discuss the work function upon the adsorption; the Figure 3.25 shows the change in work function as a function of the coverage; the experimental data are from Hrbek (1985). Although our calculations reproduce the qualitative trend with the minimum correctly the magnitude is severely underestimated, most likely due to the applied generalised gradient approximation for the exchange-correlation functional since we have seen considerable errors in work functions for the clean aluminium and ruthenium surfaces, and on all adsorbate systems studied in the present work where a comparison to experiments is possible. It is interesting to note that although the work function of the clean ruthenium surface is too low, the change in the work function for an

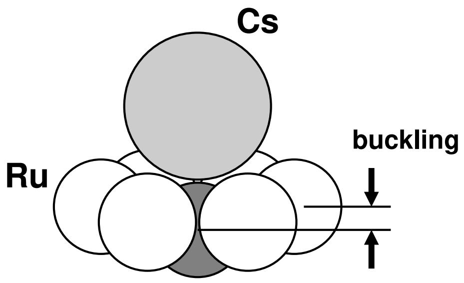

Figure 3.24: The schematic adsorption geometry of cesium at the on-top site forming a semi-seven-fold coordination

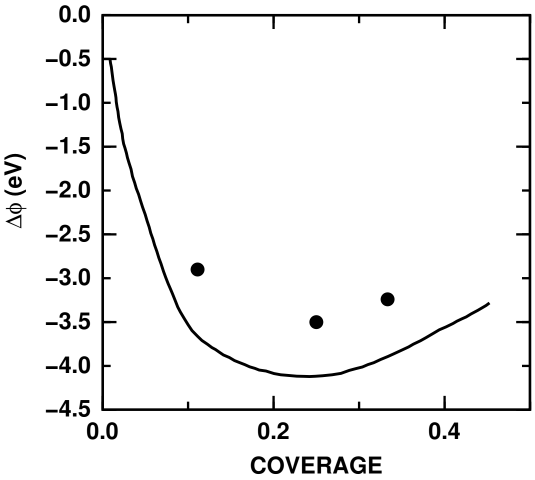

Figure 3.25: The change in the work function upon adsorption of Cs on Ru (0001); the solid line is from experiments by Hrbek (1985) and circles from our density functional calculations. At each coverage the adsorption site with largest adsorption energy was used in our results – please see the text

electropositive species like cesium is too small whereas for an electronegative species *e. g.* oxygen it is too large. Thus the work function of the surface with the adsorbate is overestimated or the too low a work function of the clean surface is responsible for the error.

The Figure 3.26 shows the change in the density upon adsorbing cesium to the surface both at the hcp and on-top site in the $(\sqrt{3}\times\sqrt{3})$R30°, (2×2) and (3×3) structures; the density of pure cesium layers needed in the differences was obtained from the superposition of a layer of cesium atoms in the corresponding cell. Common features in all of the structures are easily distinguishable, among them the most prominent is the increase of electron density in the d_{z^2} orbitals of the outer-most layer ruthenium atoms, and the decrease of the d_{xz} and d_{yz} orbitals of the same atoms. Furthermore the changes around the cesium atom are in all the cases similar, being smaller than expected from the large decrease in the work function and somewhat in a wrong direction expected if the decrease would be assigned only to the ionisation of the cesium atoms because there is for example a region of increased density above the cesium atom; this increases the dipole moment and subsequently the work function. However, the decrease in the work function is not entirely due to an “ionisation” or “charge transfer” – or rather, hybridisation of the states of the alkali and the surface – of the alkali but the work function of the surfaces of pure alkalis are about 2 eV, *i. e.* about three electron volts lower than that of Ru (0001), and the value of the work function of multi-layers of alkali on Ru (0001) should finally approach this value although in the multilayers the cesium atoms are not

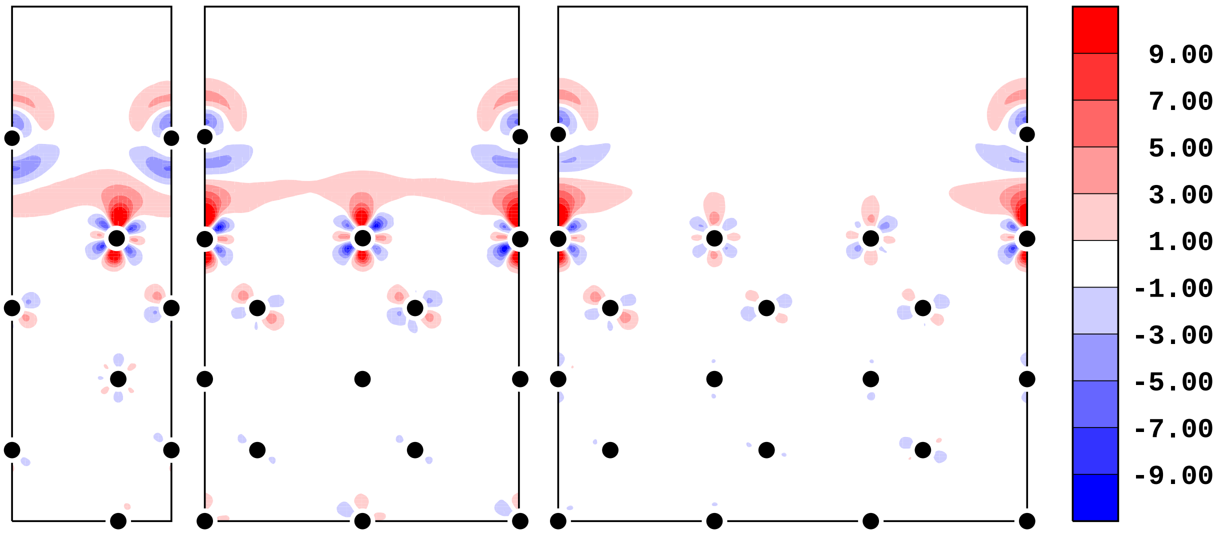

Figure 3.26: The change in the electron density upon the adsorption of Cs on Ru (0001) from our density functional calculations

ionised. We acknowledge Alberto Morgante for reminding about this consideration.

The decomposition of the charge density difference to the contribution from the 5s, 5p and valence orbitals, shown in the Figure 3.27, indicates that also the semi-core states 5s and 5p polarise strongly upon the adsorption, although their participation to the bonding is expected to be small. A close inspection, shown in the Figure 3.28, clearly reveals a bonding-like hybrid of d_{z^2} character at the nearest-neighbour ruthenium atom with the 5p orbital of the cesium atom. Even if not a bonding at least some kind of an effect of the nearest-neighbour ruthenium atom on the cesium 5p level is expected based on the orbital overlap of the two free atoms in the Figure 3.29, resulting in a Pauli repulsion with mainly the Ru_{5s} and Ru_{4d} orbitals due to the ortho-normalisation of the single-particle states.

Please notice that the large changes of an increase above the atom and a reduction below was seen to happen also with the second pseudo potential with smaller core radii for the 5s and 5p orbitals, proving that these effects are not an artifact of the pseudo potential treatment of the region close to the nuclei because in this pseudo potential were smaller than the region around the atom where the major part of the change occurs.

An indication of the charge density distribution upon adsorption can be obtained from the asymptotic behaviour of the charge density outside the surface, into the vacuum, because this is different for different surface atoms and different chemical states of the same atom because the potential depends on the electronic structure of the adsorbate and this determines the tail of the charge density into the vacuum.[2] The asymptotic densities are collected into the Figure 3.30: The (3×3) curve clearly deviates from the curves at the higher coverages, or from the curve for the free mono-layer; only the curve with the ionised cesium atom can follow the density at the low-coverage structure; however the amount of ionisation is unrealistically large.

A further measure of the asymptotic electronic structure is provided by the pseudo scanning tunnelling microscope images in the Figure 3.31, calculated using the Tersoff-Hamann model introduced in the Section 2.5.11. At the clean surface the corrugation is negligible, and a large

[2] Please note that the generalised gradient approximation yields an incorrect decay of the potential into the vacuum; we hope that the qualitative behaviour is correctly reproduced, which is likely since the geometry, work function *etc* are well described within our current approach

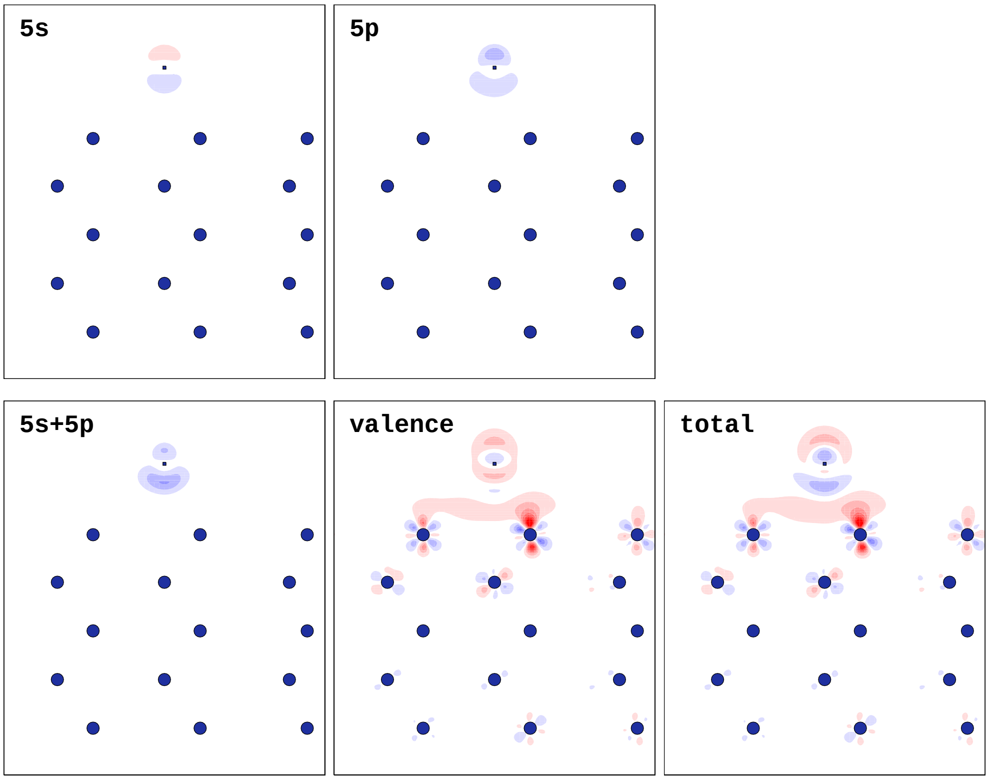

Figure 3.27: The change in the electronic density of the Cs_{5s} – upper left panel –, Cs_{5p} – upper middle –, sum of Cs_{5s} and Cs_{5p} – lower left –, valence energy region – lower middle – and the total density – lower right – upon the adsorption of Cs on Ru (0001) in the (3×3) structure from our density functional calculations

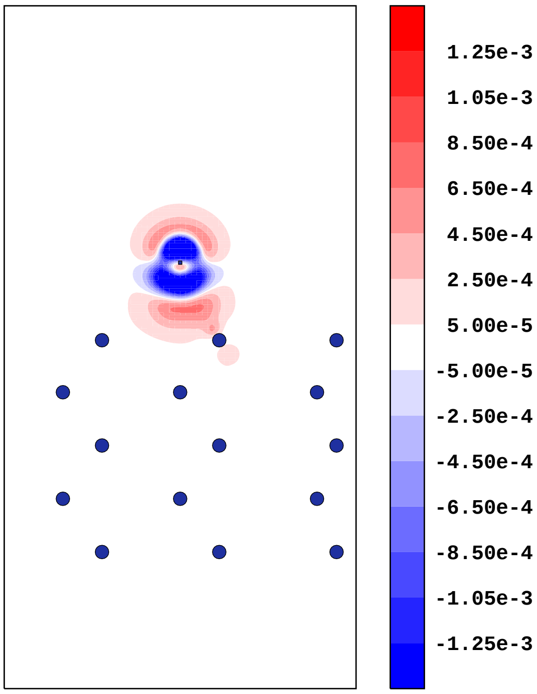

Figure 3.28: The change in the electronic density of the Cs_{5p} energy region upon the adsorption of Cs on Ru (0001) in the (3×3) structure; this is the same figure as the middle panel in the upper row of the Figure 3.27 but on a finer scale

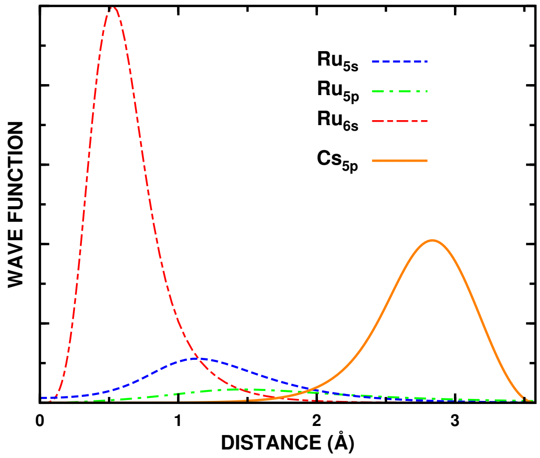

Figure 3.29: An illustration of the orbital densities from free-atom wave functions of ruthenium and their overlap with the semi-core state 5*p* of a cesium atom; the distance between the ruthenium and cesium atoms is taken as a typical bond length of cesium on the Ru (0001) surface

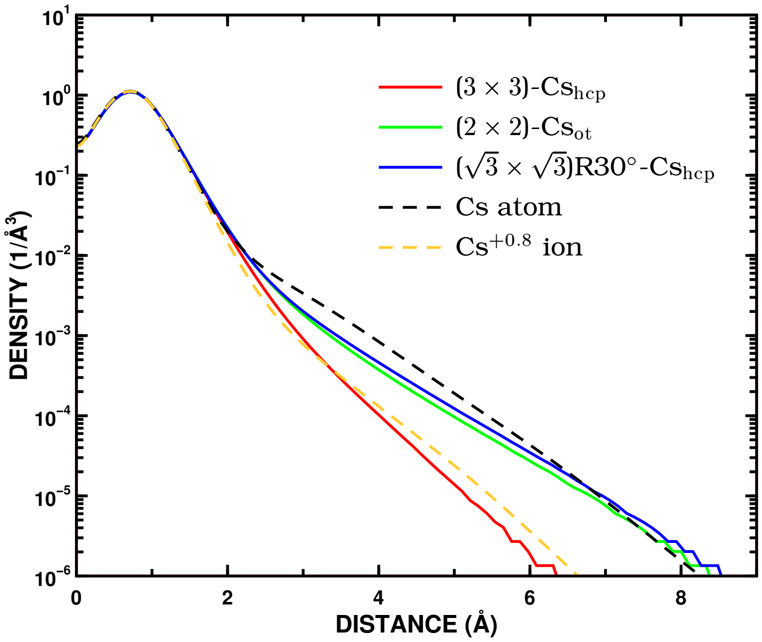

Figure 3.30: The asymptotic density above the cesium atom in different structures on the Ru (0001) surface as obtained in our calculations. The black and orange dashed lines are the asymptotic densities of a neutral cesium atom and a cesium ion with the net charge of +0.8 of the absolute of the charge of an electron, respectively; the blue, green and red lines are the densities in the $(\sqrt{3} \times \sqrt{3})R30°$, (2×2) and (3×3) structures

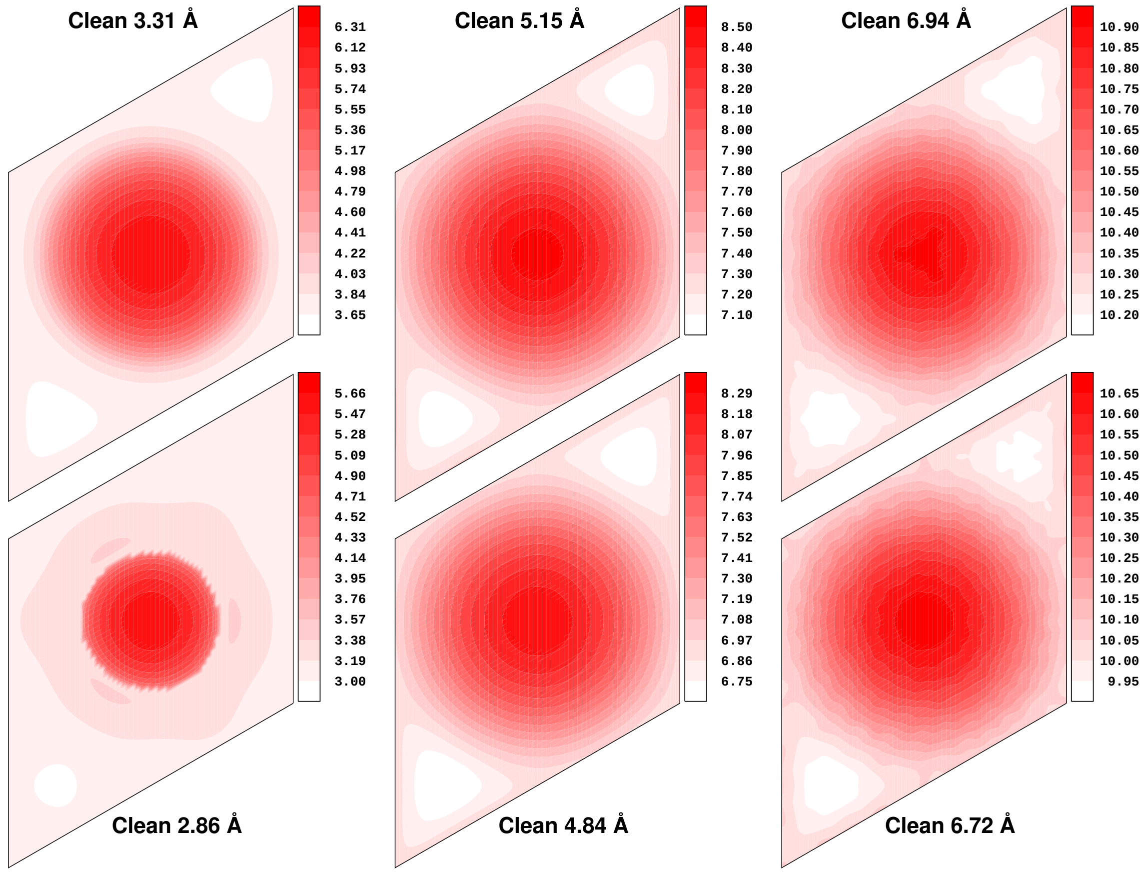

Figure 3.31: The pseudo scanning tunnelling microscope images produced via the Tersoff-Hamann model for cesium at the hcp site on the Ru (0001) surface in a (3×3) geometry using our calculated Kohn-Sham orbitals. In the upper panel the total density and in the lower the density arising from the Kohn-Sham states $\pm 1/2$ eV around the Fermi energy was used, and shown is the distance – in Ångströms – from the upper-most ruthenium layer in the constant density mode with the values 10^{-4}, 10^{-6} and 10^{-8} e^-/Bohr^3 from the left-most to the right-most panel; the corresponding average distances at the clean surface are indicated

corrugation and a distance much larger than at a clean surface is immediately obvious. This is of course as expected since the loosely bound 6*s* electron decays slowly into the vacuum, causing the density to be increased by a small but sufficient amount. Except for the largest tunnelling current *i. e.* largest electron density in the left-most panels in the Figure 3.31 the corrugation extracted from the plot for the total density or the density in the vicinity of the Fermi level only are very similar; this is because the major effect of the adsorption of cesium on the surface happens in the neighbourhood of a couple of electron volts around the Fermi energy as we shall discuss below. Qualitatively the effect is so large that changing the electron density and thus the tunnelling current by four orders of magnitude does not lead to qualitative changes beyond the apparently smaller size of the bump around cesium; only at the largest tunnelling currents would the tip approach the surface to the same distance as at the clean surface. Since the coverage was only 1/9 in these images this is a clear indication of the large effective size of the adsorbed cesium and in higher coverages the corrugation would decrease – also due to the increased metalicity – and the tip would remain still further from the surface even at the minima.

An useful concept to investigate the distribution of the charge density upon the adsorption of an alkali metal is the induced density, which was discussed in the Section 2.5.8 and used *e. g.* by

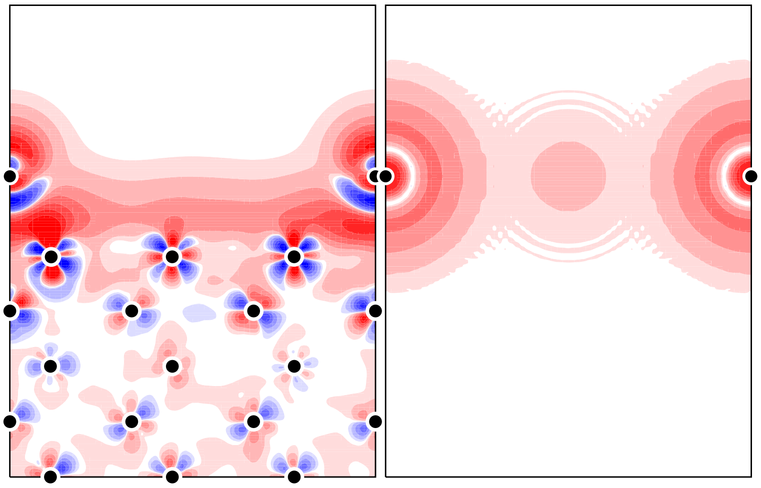

Figure 3.32: The charge density induced by the adsorption of cesium in the Ru (0001)-(3 × 3)-Cs_{hcp} structure – left – and the superposition of the charge densities from free cesium atoms in the same cell – right

Neugebauer and Scheffler (1992). Please notice that if the 6*s* orbital of the free atom would also be subtracted this would be equal to the ordinary density differences. Therefore qualitatively the induced density describes where the 6*s* is located in the adsorbed system and how the electron density has changed during the interaction. The induced density in the Ru (0001)-(3 × 3)-Cs_{hcp} structure is compared face to face against the super-imposed charge densities from free cesium atoms in the Figure 3.32. The shapes are reminiscent, with the spherical shape above the atoms and a region of density in between the subsequent cesium atoms, but especially the radial density is largely contracted; also in the region between the cesium atoms the density above the line connecting the alkali atoms undergoes a slight reduction. Therefore qualitatively the alkali decreases in size and donates part of its long-range tail of the 6*s* orbital most likely to the hybrids with the surface; but most importantly, the long range of the 6*s* orbital would cause a large Pauli repulsion with the surface atoms and thus the character of the orbital must be changed and a partial ionisation alone would not suffice to eliminate the repulsion, only a complete ionisation of the cesium can prevent the repulsion. These observations lead to a qualitative picture like in the Figure 3.33 where the density of the 6*s* orbital is reduced, mostly by a shift from below the atom and from the long range towards the nucleus. It is important to realise that also in the higher coverages the 6*s* orbital has to face the repulsion with the surface electron, independent whether the atom would or would not be ionised, as the distance from the surface atoms hardly varies with the coverage. The induced charge density in the Figure 3.34 for the Ru (0001)-(2 × 2)-Cs_{ot} structure indicates how the apparent size of the cesium atom has now increased relative to the lower-coverage structure and between the cesium atoms the density remains higher throughout the surface unit cell, with the smallest contour staying almost at constant height. This is naturally exactly what was expected to happen in the pseudo scanning tunnelling microscope images: the corrugation would be small and the tip would reside at remarkable heights from the ruthenium atoms at the surface.

The electro-static potential is shown in the Figure 3.35 for the clean Ru (0001) surface and with the adsorbed cesium in an (3 × 3) over-layer, with their difference in the panel on the right; this is the electro-static potential created by the induced density of the cesium atom since the electro-static potential is a linear operator. The difference shows how fast the changes in the electronic structure

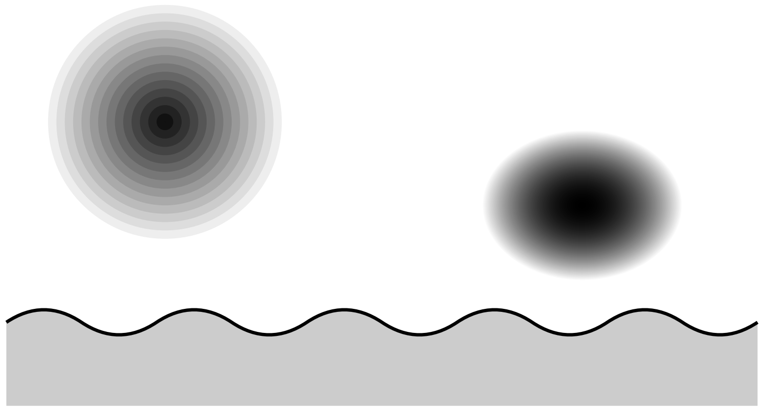

Figure 3.33: The schematic change in the 6*s* orbital upon adsorption; the atomic state at left is before and at right – deformed and split among many hybrids with the states of the substrate – after the adsorption: The hybrids formed upon adsorption are more localised especially vertically since the weak potential into the vacuum and strong Pauli repulsion with the states of the substrate oppress the states from both sides

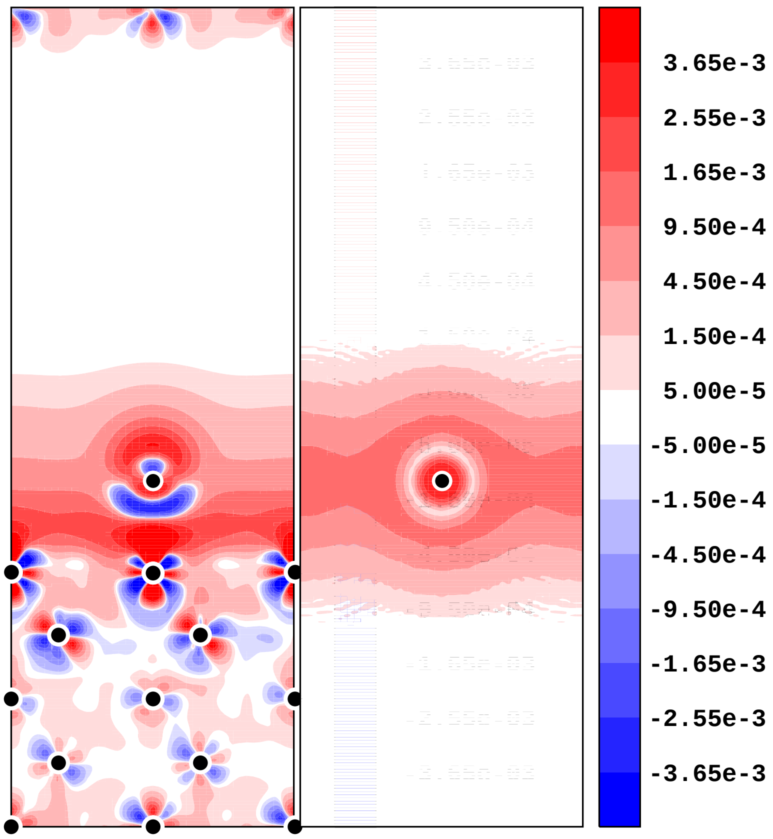

Figure 3.34: The charge density induced by the adsorption of cesium in the Ru (0001)-(2 × 2)-Cs_{ot} structure – left – and the superposition of the charge densities from the 6*s* orbitals from free cesium atoms in the same cell – right

due to the alkali metal are screened towards the bulk of the slab, and this also validates that the thickness of our slab is sufficient to treat the adsorption of the alkali metal. The difference has been normalised to zero in the vacuum of the side of the clean surface of the slab, and thus the difference gives us the change in the work function, and now it can be studied varying in space whereas the usual definition of the work function is an integral over the region parallel to the surface. The lateral variation has been studied experimentally with the method of the photo-emission of adsorbed xenon – *PAX* – (Wandelt, 1987), where the xenon atoms experience a different electro-static potential depending on the adsorption site and thus their polarisation and subsequently the electron binding energy depends on the local environment around the xenon atoms. Wandelt and co-workers have applied this method to several cases of alkalis adsorbed on metal surface, and the results (Markert & Wandelt, 1985) for potassium adsorbed on the Ru (0001) surface are reproduced in the Table 3.5. Unfortunately we have not studied the adsorption of potassium on this surface at low coverages, and the lowest coverage we have studied with cesium is only the largest coverage of potassium in the investigations of Markert and Wandelt, and the cesium is furthermore larger than the potassium. Despite these differences we found it interesting to make a comparison to these experiments, and to approximate the value of the "local work function", as termed by Wandelt and co-workers, we determined the adsorption height by taking the density at a clean Ru (0001) surface corresponding to the adsorption height in the Ru-($\sqrt{3} \times \sqrt{3}$)R30°-Xe$_{\mathrm{ot}}$ structure; the height from our calculations (Ari P Seitsonen, unpublished results) – 4.09 Å with the generalised gradient approximation – is much larger than the experimental value of 3.54 Å by Narloch and Menzel (1997); our value with the local density approximation is in turn too small, 2.84 Å. However, we continue to use the value from the generalised gradient approximation since a slight error in the density will not lead to qualitative changes in the final results of our studies. This gives us the density 1.02×10^{-4} Å^{-3} in which the xenon atom likes to reside, and with this density we obtain the map of the local work function in the Figure 3.36, and from this data we extract the approximate work function in the Table 3.5. We acknowledge the drastic approximations made in our estimation, but the qualitative agreement with the experimental results gives some creditability to the procedure. We find about the same value of the work function for cesium as was obtained in experiments for potassium, being in agreement with the too small a change in the calculation as shown in the Figure 3.25. We took the value for the xenon adsorbing at the surface under the influence of alkali – Xe/A/Ru – from the site furthest away from the alkali in the unit cell; for the adsorption at the clean surface – Ru – our coverage 1/9 is still too large and unit cells (4×4) and beyond should be used.

It is instructive to compare the change in the electro-static potential at the Ru (0001) surface to the corresponding change at a jellium surface, as shown in the Figure 3.37 together with the change in the electron density in both cases; a (2×2) cell was used. The qualitative change is obvious, although the potentials somewhat differ.

The electro-static potential, or rather the changes in it, give rise to electric fields which then influence the electrons of the co-adsorbates; the electric field is the negative gradient of the electro-static potential,

$$E = -\nabla V_{\mathrm{els}} \ . \tag{3.3}$$

The field is a vector quantity and has thus three components; in order to represent the results in a clear way we show either the three components separately or show only the magnitude of the field, and since we are interested in the changes in the electric field caused by the cesium we use cylindrical coordinate system for the gradient where the vertical axis goes through the centre

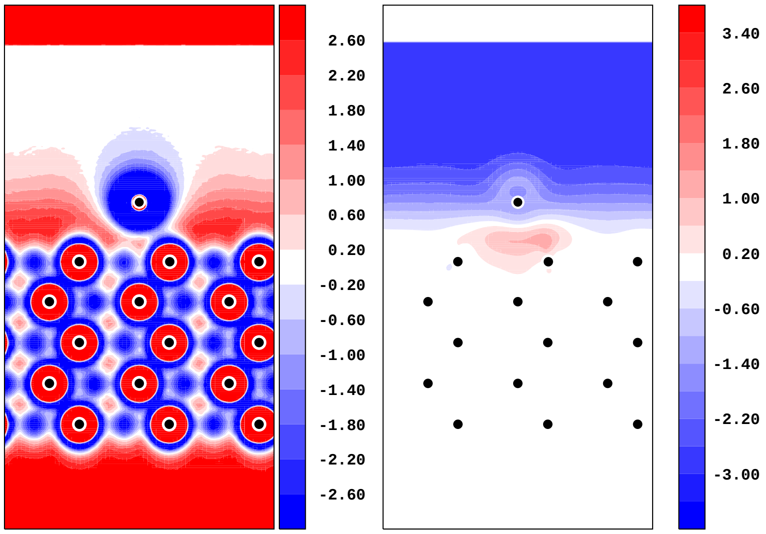

Figure 3.35: The electro-static potential of the system Ru (0001)-(3 × 3)-Cs_{hcp} – left – and the change in electro-static potential relative to the clean surface – right

Table 3.5: The local work function at different sites for potassium from experiments (Markert & Wandelt, 1985) and cesium from density functional calculations on th Ru (0001) surface; the process of determining the value from the calculation is described in the text. $\phi(\mathrm{Xe/Ru})$, $\phi(\mathrm{Xe/A/Ru})$ and $\phi(\mathrm{Xe/A})$ are the work function at the patches of the clean surface, at the surface next to the alkali and above the alkali atom, respectively. All entries are in electron volts

	θ(A)	$\phi(\mathrm{Xe/Ru})$	$\phi(\mathrm{Xe/A/Ru})$	$\phi(\mathrm{Xe/A})$
	0	5.52	—	—
	K: 1/60	5.44	4.89	4.17
Experiments	K: 1/30	5.17	4.54	3.77
	K: 1/15	5.02	4.19	3.27
	K: 1/10	—	3.86	2.97
Calculations	Cs: 1/9	—	2.67	1.89

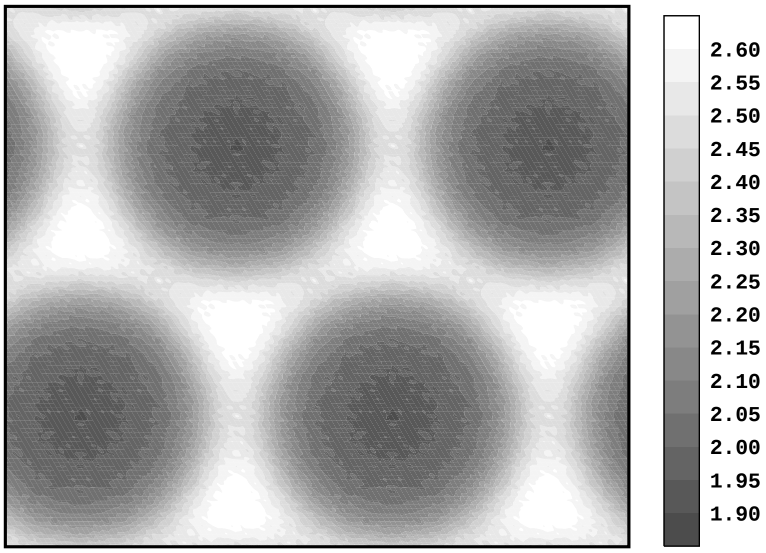

Figure 3.36: The local work function in the structure Ru (0001)-(3 × 3)-Cs_{hcp}; the values are in electron volts. Please refer to the text for details about the evaluation of the local work function. The cesium atoms reside below the minima of the work function

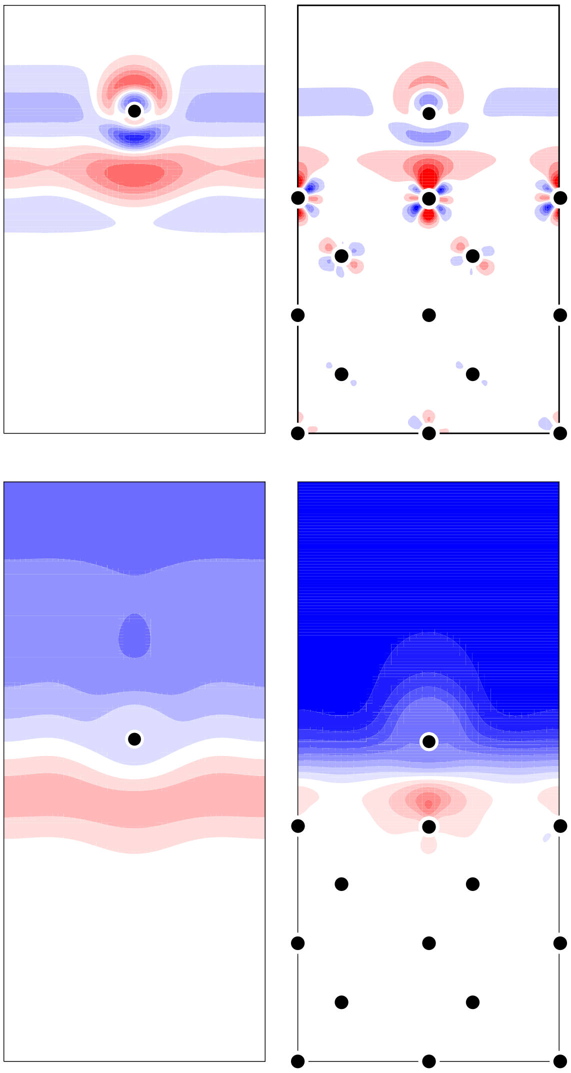

Figure 3.37: The change in the electron density – upper panels – and electro-static potential – lower panels – upon the adsorption of cesium on a jellium surface – left – and on the Ru (0001) surface – right – in the (2 × 2)-Cs_{ot} structure. The density parameter of the jellium slab was $r_s = 3$ Bohr

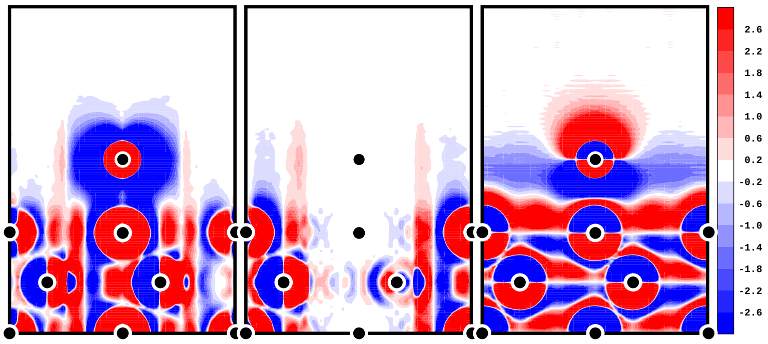

Figure 3.38: The radial, azimuthal and vertical components of the electric field – from left to right, in electron volts per Ångström – arising from the electro-static potential in the Ru (0001)-(2×2)-Cs_{ot} structure

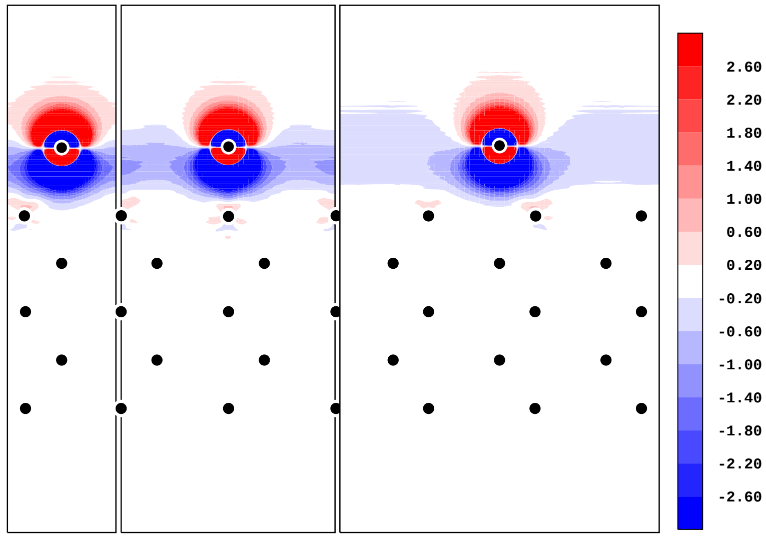

Figure 3.39: The change in the vertical component of the electric field induced upon the adsorption of cesium in the $(\sqrt{3} \times \sqrt{3})$R30°-$Cs_{hcp}$, (2×2)-Cs_{ot} and (3×3)-$_{hcp}$ structures, from left to right. All the fields are in electron volts per Ångström

of the cesium atom, along the surface normal; thus we have the radial, azimuthal and vertical components of the field like in the Figure 3.38 for cesium in the (2×2)-Cs_{ot} structure. In this case the vertical component is clearly dominating the lateral field, and thus the magnitude of the field is approximately the magnitude of the vertical field, being about 1.7 eV/Å; this is in a good agreement with the simple kind of prediction by Mortensen *et al* (1997): from the change in the potential of −3.5 eV in the work function over a distance of about ≈2 Å the estimated field would be −1.7 eV/Å. These are strong fields on the molecular scale. In the Figure 3.39 the vertical component of the electric field at the surface shows a clear reduction as a function of coverage, being only 0.9 eV/Å in the lowest coverage furthest away from the cesium.

We now come to study the electronic structure of the cesium over-layer and its bonding to the substrate in more detail using the calculated change in the total density of states in the Figure 3.40 and the projected density of states at the site of the cesium atom at different adsorption sites in the Figure 3.41 and as a function of coverage in the Figure 3.42. The change in the total density of states shows little difference between the two different adsorption sites studied in the low coverage, and overall rather a small dependence on the coverage; there are two dips, at 5.5 eV below and

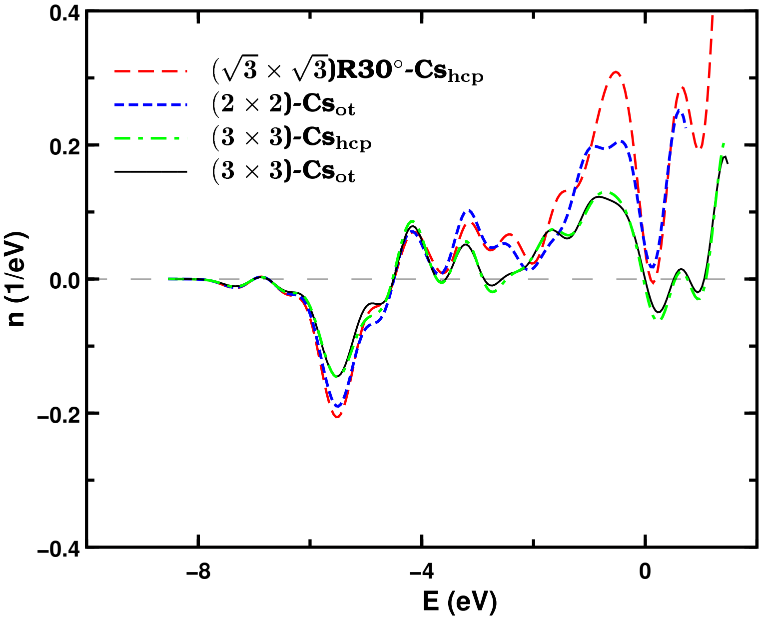

Figure 3.40: The change in the total density of states – calculated from the Kohn-Sham eigenvalues – due to the adsorption of cesium on the Ru (0001) surface

0.5 eV above the Fermi energy, and an increase between these two energies and above the dip at 0.5 eV. In the projected density of states at the cesium atom the magnitude of the *s* component grows from 4 eV below the Fermi energy, having a peak and a dip at half of an electron volt below and above the Fermi energy, corresponding qualitatively the change in the total density of states; however, the dip at low energy and the depth of the peak at just above the Fermi energy remain unexplained, although we expect the former to be an artifact of changes at the other, clean surface of the slab. The difference between the hcp and on-top sites is small, but at 2 eV below the Fermi energy there appears a peak which is present only in configurations with the cesium at the hcp site; in the geometries with the cesium on the on-top site there is a corresponding, though weaker, increase in the $d_{xz,yz}$ orbitals. Also the peak in the d_{z^2} is in lower energies at the on-top than at the hcp site; otherwise the magnitude of the *s* component clearly scales with the cesium coverage whereas the *p* components do not.

In the Table 3.6 we have collected the density of states projected at the site of the cesium, multiplied with the Fermi occupation function as in our self-consistent calculation and then integrated over the energy. Thus the values resemble the number of electrons with the corresponding angular quantum numbers but the magnitude should not be taken too seriously, rather the changes in the magnitude, due to the considerations mentioned in the Section 2.5.4. For cesium we used the 5*p* wave function for all the *p*-like electrons and the 6*s* wave function for both the semi-core and valence *s*-like orbitals although the latter is largely changed due to the influence of the surface; please see the Figure 3.33. Beyond this the change in the *p* and *d* orbitals is small at different coverages and adsorption sites but the magnitude of the *s* component increases, most likely since due to the metallisation of the valence electrons, which leads to a recovery of the more atomic-like 6*s* orbital. It is also interesting to notice that the 5*d* orbitals at the cesium site are indeed somewhat filled at the surface like we found to occur also in a free mono-layer of cesium, whereas they are empty in the free atom. However they lie only about −1.7 eV above the 6*s* orbital in the free atom and can thus become easily occupied in a suitable environment.

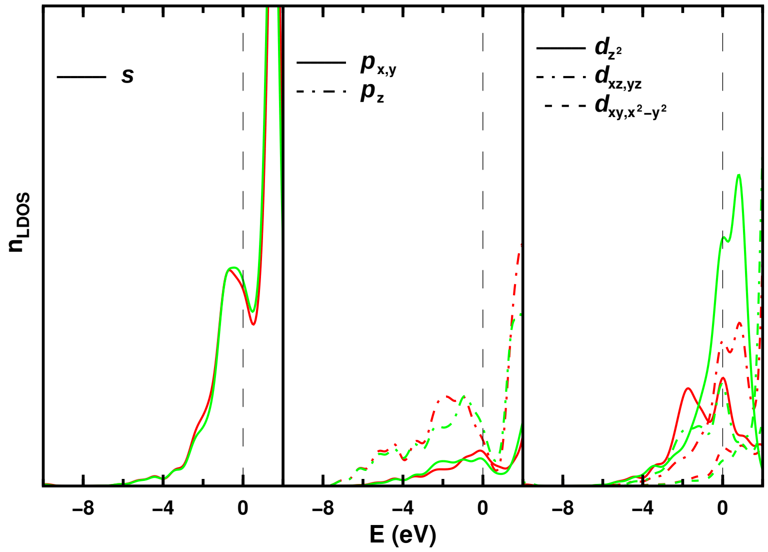

Figure 3.41: The local density of states projected to the cesium atom in the Ru (0001)-(3 × 3)-Cs_{hcp} – red – and Ru (0001)-(3 × 3)-Cs_{ot} structures – green

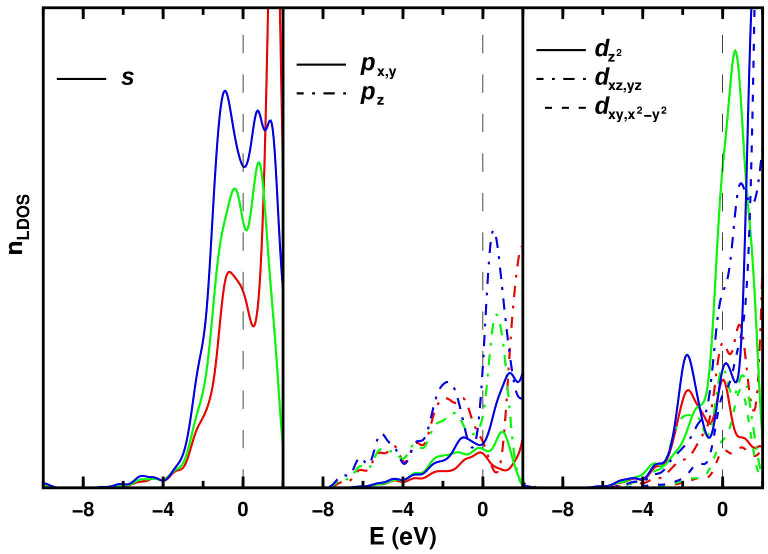

Figure 3.42: The local density of states projected to the cesium atom in the Ru (0001)-($\sqrt{3}\times\sqrt{3}$)R30°-Cs_{hcp} – blue –, Ru (0001)-(2 × 2)-Cs_{ot} – green – and Ru (0001)-(3 × 3)-Cs_{hcp} – red – structures

Table 3.6: The integral of the density of states projected on the cesium atom at different coverages and adsorption sites

System	s	$p_{x,y}$	p_z	d_{z^2}	$d_{xz,yz}$	$d_{x^2-y^2,xy}$
Ru-($\sqrt{3}\times\sqrt{3}$)R30°-Cs_{hcp}	0.30	1.79	1.78	0.03	0.02	0.01
Ru-(2 × 2)-Cs_{ot}	0.28	1.79	1.78	0.03	0.02	0.01
Ru-(3 × 3)-Cs_{hcp}	0.26	1.79	1.79	0.03	0.02	0.00
Ru-(3 × 3)-Cs_{ot}	0.26	1.79	1.78	0.03	0.02	0.00

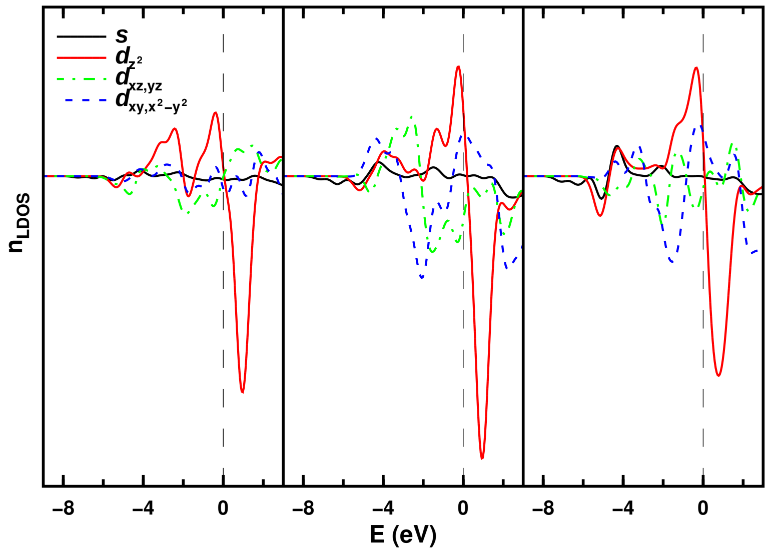

Figure 3.43: The change upon the adsorption of cesium onto Ru (0001) in the density of states projected on the orbitals of the nearest-neighbour ruthenium atom of the cesium as a function of the coverage; the structures are Ru (0001)-($\sqrt{3} \times \sqrt{3}$)R30°-Cs$_{\rm hcp}$ – left –, Ru (0001)-(2 × 2)-Cs$_{\rm on-top}$ – middle – and Ru (0001)-(3 × 3)-Cs$_{\rm hcp}$ – right. The *p* orbitals have been neglected due to their small magnitude because they were projected on the radial wave function of the semi-core 5*p* state

The ruthenium atoms in the surface layer showed characteristic features upon the adsorption of cesium: firstly there is a region of increased charge above the first layer between the surface atoms, and secondly the *d* orbitals of the surface atoms polarise strongly. Whereas the former is due to weakly bound and long-tail electronic states, the latter is localised around the ruthenium atoms and thus it can be clearly seen in the projected density of states; this is shown in the Figure 3.43 as the change from a clean surface for the different coverages, together with this change multiplied by the Fermi occupation statistics and integrated over the energy in the Table 3.7. The most prominent effect is the filling of the d_{z^2} orbitals just above the Fermi energy by moving them downwards in the energy, thus causing an increase in the integral over the projected density of states. Especially in the lower coverages the other *d* orbitals have a double peak structure with a decrease between them. The *s* and *d* orbitals have a component along the z axis have a small dip at -5.5 eV below the Fermi energy where the dip was found also in the change of the total density of states.

An interesting feature in the change of the projected density of states is how similar especially the d_{z^2} orbitals are in spite of the different coverage and even adsorption site of the cesium. Therefore we extracted the change in the density of states projected on the different ruthenium surface atoms for the same system – Ru (0001)-(3 × 3)-Cs$_{\rm on-top}$ as there the distance from the cesium to the nearest neighbour ruthenium atom is one of the shortest and the distance to the next-next nearest neighbour is the largest in the systems studied here – and the result is given in the Figure 3.44. The similarity at the different distances is obvious although the largest distance, from the cesium to the third-nearest neighbour, is 2.56 Å or 80 % longer than the shortest one from the cesium to the ruthenium below it, and the angle to this atom is 56° from the direction to the nearest-neighbour ruthenium atom beneath the cesium. To test the idea of scaling with the distance we multiplied the change in the projected density of states with the distance from the cesium atom, with the result in the Figure 3.45 for the d_{z^2} orbital and in the Table 3.8 for all the different angular functions integrated over the energy. The scaling is very close to linear in the distance especially in the d_{z^2}

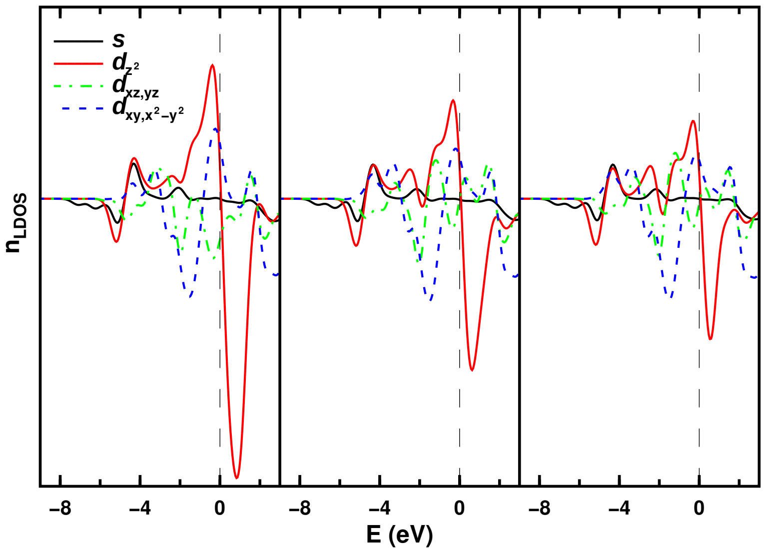

Figure 3.44: The change upon the adsorption of cesium into the Ru (0001)-(3 × 3)-Cs_{on-top} structure in the density of states projected on the orbitals of the nearest-neighbour – left –, next-nearest neighbour – middle – and next-next-nearest neighbour – right – ruthenium atom of the cesium. The projection onto the p orbitals has been neglected

orbital and reasonable in the other d orbitals.

As the cesium is adsorbed on the surface the coordination of the ruthenium atoms on the surface increases and thus the centre and width of the d band are expected to approach the values in the bulk, thus the position of the centre should become deeper in energy and the width increase. This is just what is seen to happen in the Table 3.9, although the changes do not yet recover the bulk values; changes of −0.2 eV and +0.5 eV in the position of the centre and width of the d band, respectively, would be necessary to achieve this.

We finally studied the change in the $5p$ eigenvalues of cesium as a function of coverage in order to estimate to what extent they participate to bond formation directly and indirectly via the change of the potential upon adsorption. We show in the Figure 3.46 the binding energies from the $5p$ Kohn-Sham eigenvalues and ultra-violet photoemission spectra by Hrbek (1985). The theoretical Cs_{5s} and Cs_{5p} eigenvalues are given in the Table 3.10, where the values are given at the **k** points used in the self-consistent calculations. The deviation in the points arises from eigenvalues at different **k** points and shows the dispersion of the bands and thus illustrates the amount of interaction, whereas the change in the average position is due to the adsorbate-substrate interaction.

One immediate discrepancy in the experimental and theoretical values arises, beyond a shift in the magnitude: The Kohn-Sham eigenvalues shift downwards in energy with increasing coverage whereas the experimental binding energies decrease, after the initial increase at low coverages. This could be due to several effects, like the final-state relaxation effects which would lower the binding energies, the inadequency of the Kohn-Sham eigenvalues to predict real excitation energies or the use of the generalised gradient approximation in our calculations instead of the exact exchange-correlation functional.

Modelling of alkali adsorption via an electric field As we saw above the adsorption of the alkali metal induces an electro-static potential above the surface, with a magnitude in the excess of one electron volt in the (2 × 2) arrangement of the adsorbates. We thus calculated the response of the

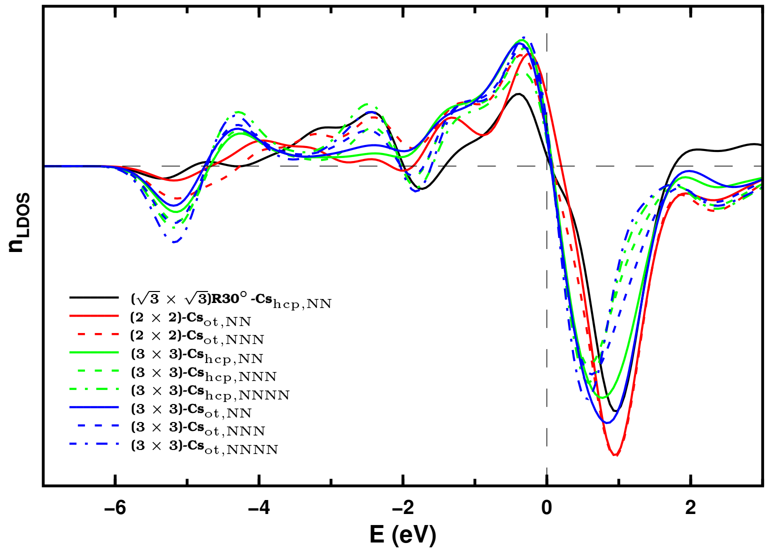

Figure 3.45: The change in the density of states projected on the d_{z^2} orbital of the surface ruthenium atoms at the different coverages and adsorption sites upon the adsorption of cesium onto the Ru (0001) surface

Table 3.7: The change in the integral of the density of states projected on the ruthenium atoms at the surface layer; nn, nnn and nnnn correspond to the nearest, next-nearest and next-next-nearest ruthenium surface atom from the cesium. The last column shows the distance of the cesium and the ruthenium atoms

System	Atom	s	$p_{x,y}$	p_z	d_{z^2}	$d_{xz,yz}$	$d_{x^2-y^2,xy}$	d (Å)
Ru-$(\sqrt{3}\times\sqrt{3})$R30°-Cs$_{hcp}$	Ru(nn):	+0.001	+0.002	+0.005	+0.074	−0.048	+0.001	3.50
Ru-(2×2)-Cs$_{ot}$	Ru(nn):	+0.008	+0.003	+0.005	+0.103	−0.041	−0.047	3.16
	Ru(nnn):	+0.002	+0.000	+0.003	+0.093	−0.049	−0.045	4.19
Ru-(3×3)-Cs$_{hcp}$	Ru(nn):	+0.005	−0.001	+0.004	+0.104	−0.032	−0.028	3.58
	Ru(nnn):	+0.003	−0.001	+0.002	+0.074	−0.023	−0.026	4.53
	Ru(nnnn):	+0.004	−0.000	+0.002	+0.064	−0.018	−0.026	5.31
Ru-(3×3)-Cs$_{ot}$	Ru(nn):	+0.007	+0.000	+0.005	+0.128	−0.040	−0.028	3.22
	Ru(nnn):	+0.003	−0.001	+0.003	+0.086	−0.031	−0.025	4.25
	Ru(nnnn):	+0.003	−0.002	+0.002	+0.063	−0.014	−0.030	5.79

Table 3.8: The change in the integral over the density of states on the surface ruthenium atoms upon the adsorption of cesium scaled with the distance from the cesium atom

System	Atom	s	$p_{x,y}$	p_z	d_{z^2}	$d_{xz,yz}$	$d_{x^2-y^2,xy}$
Ru-($\sqrt{3}\times\sqrt{3}$)R30°-Cs_{hcp}	Ru(nn):	+0.00	+0.01	+0.02	+0.26	−0.17	+0.00
Ru-(2 × 2)-Cs_{ot}	Ru(nn):	+0.03	+0.01	+0.02	+0.33	−0.13	−0.15
	Ru(nnn):	+0.01	+0.00	+0.01	+0.39	−0.21	−0.19
Ru-(3 × 3)-Cs_{hcp}	Ru(nn):	+0.02	−0.00	+0.01	+0.37	−0.11	−0.10
	Ru(nnn):	+0.01	−0.01	+0.01	+0.33	−0.10	−0.12
	Ru(nnnn):	+0.02	−0.00	+0.01	+0.34	−0.10	−0.14
Ru-(3 × 3)-Cs_{ot}	Ru(nn):	+0.02	+0.00	+0.02	+0.41	−0.13	−0.09
	Ru(nnn):	+0.01	−0.00	+0.01	+0.37	−0.13	−0.11
	Ru(nnnn):	+0.02	−0.01	+0.01	+0.36	−0.08	−0.17

Table 3.9: The change in the centre and width of the d band upon the adsorption of cesium and when applying an electric field with a magnitude of 0.4 eV/Å on the slab

Structure	Site	Coverage	Atom	$\bar{E}_d$ (eV)	W_d (eV)
($\sqrt{3}\times\sqrt{3}$)R30°	hcp	1/3	NN	−0.04	0.15
(2 × 2)	on-top	1/4	NN	−0.14	+0.13
			NNN	−0.05	+0.08
(3 × 3)	hcp	1/9	NN	−0.06	+0.07
			NNN	−0.04	+0.08
(3 × 3)	on-top	1/9	NN	−0.08	+0.10
			NNN	−0.05	+0.09
E_{field}				−0.01	+0.01

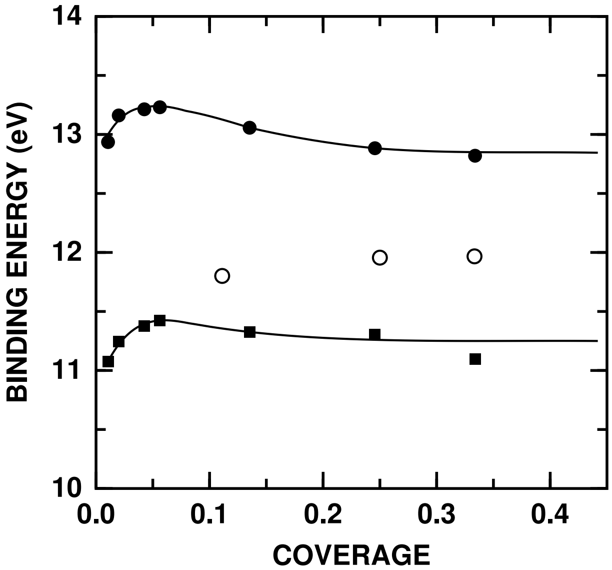

Figure 3.46: The binding energies of the 5p orbitals from ultra-violet photoemission spectra and the Kohn-Sham eigenvalues of cesium on Ru (0001) at different coverages; the filled symbols are from experiments by Hrbek (1985), split due to spin-orbit coupling, and the open symbols from the calculations, the latter being shifted two electron volts to larger binding energies to improve comparability

Table 3.10: The Kohn-Sham eigenvalues – in electron volts – corresponding to the 5s and 5p orbitals of cesium at different coverages absorbed on the Ru (0001) surface. The ranges corresponds to the dispersion of the eigenvalues at the **k** points at different regions of the Brillouin zone

Structure	Site	Coverage	Cs_{5s}	Cs_{5p}
$(\sqrt{3} \times \sqrt{3})R30°$	hcp	1/3	23.1	9.8–10.1
	on-top		23.2	9.9–10.2
(2×2)	hcp	1/4	23.0	9.9–10.0
	on-top		23.1	9.9–10.0
(3×3)	hcp	1/9	23.0	9.8–9.8
	on-top		23.0	9.8–9.9

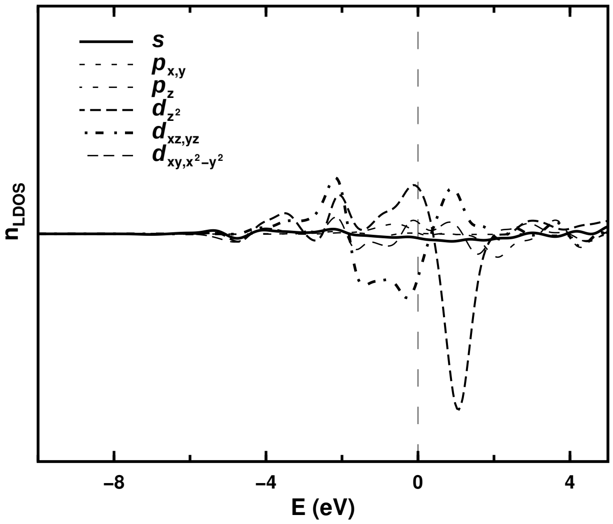

Figure 3.47: The difference in the density of states projected on the ruthenium atoms on the opposite surfaces of the Ru (0001) slab upon the application of a vertical electric field of 0.4 eV/Å

clean Ru (0001) surface and a jellium with $r_s = 3$ Bohr to an electric field. The projected density of states in the Figure 3.47, the change in the lateral – the Figure 3.48 and vertical – the Figures 3.49 and 3.50 – density and potential all resemble the changes seen above upon the adsorption of cesium onto the surface. Therefore it is beguiling to assign the effects of the alkali metal to the electric field arising from it, without any chemical binding being necessary. Yet it might be important to achieve the polarisation of the alkali atom which then gives rise to the electric field.

We further compare the change in the electron density and electro-static potential of a jellium slab with r_s=3 Bohr in the Figure 3.51. It is not very useful to compare this to the result for the Ru (0001) in the Figure 3.50 since in the latter the polarisation of the d orbitals mostly hides the change in the s and p electrons; it is more useful to compare the values with the regions above the fcc or hcp adsorption sites in the Figure 3.48. There the maximal change is about 3×10^{-4} e$^-$/Å^3, whereas it is only about 3×10^{-5} e$^-$/Å^3 on the jellium surface although the electric field has the same magnitude in both cases. Therefore we conclude that the electric field is much faster screened off on the jellium surface.

Other cases of alkali adsorption We shortly studied other cases of alkali adsorbed on the close-packed surfaces of transition metals. The main results are shown in the Table 3.11, and

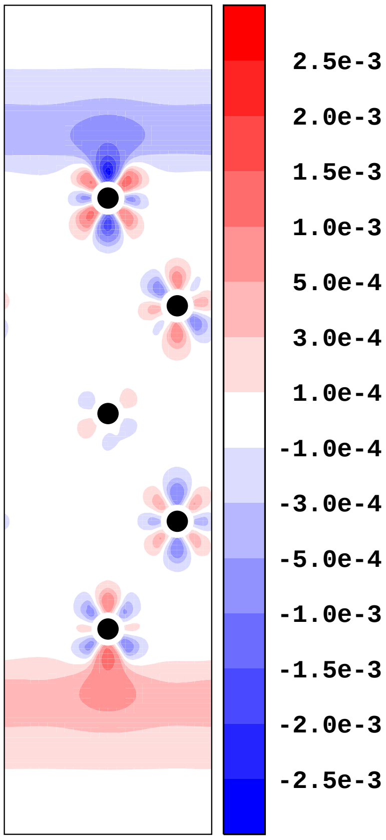

Figure 3.48: The change in the electron density of a Ru (0001) slab upon the application of a vertical electric field of 0.4 eV/Å

for some of the systems we show the density difference in the Figure 3.52. The calculations for Na/Rh (111) were performed with two substrate layers only because we only wanted to obtain a qualitative picture of the adsorption quickly. The density difference for K/Pt (111) looks very similar to the case of Cs/Ru (0001), but sodium on either platinium or rhodium – not shown – appears as qualitatively different; this is mainly due to the semi-core states of cesium and potassium, which are included as active states in these pseudo potentials, whereas in sodium the semi-core states were incorporated to the core and can thus not polarise at the surface. This choice of semi-core and valence is justified with the energetically deeper position of $2s$ and $2p$ states in sodium than of the corresponding states in potassium or cesium. Thus we believe this to be a real effect, and be due to the different chemical character of the sodium.

3.3.2 Adsorption of carbon monoxide on Ru (0001)

The adsorption of carbon monoxide on surfaces of transition metals has been studied by many experimental methods and semi-empirical and electronic structure methods – please see *e. g.* Over (1998) and references therein. On some of the transition metals – those on the left hand side of the periodic table – CO adsorbs dissociatively whereas on the surfaces of transition metals at the middle of the periodic table CO adsorbs molecularly. The adsorption on ruthenium and rhodium for example is molecular, with the molecular axis parallel to the surface normal (Dowben, 1997). Earlier, before the appearance of even qualitative studies using the low energy electron diffraction, the adsorption site was concluded mainly from the internal vibration C–O, a vibration at 1950 – 2100 cm^{-1} assigned to a one-fold on-top position, 1800 – 1950 cm^{-1} to two-fold bridge site and

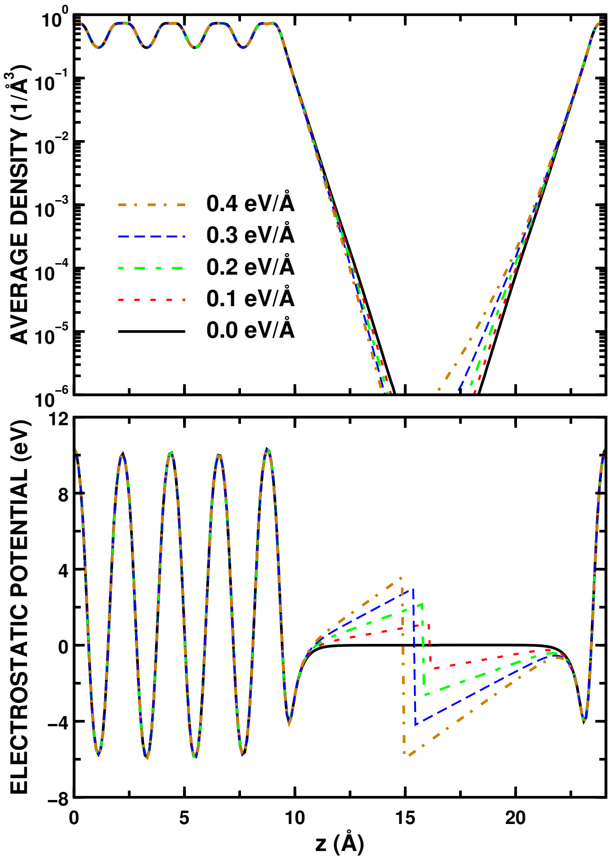

Figure 3.49: The vertical density and electro-static potential averaged parallel to the surface in a Ru (0001) slab upon the application of a vertical electric field of 0 eV/Å – solid, black line –, 0.1 – red –, 0.2 – green –, 0.3 – blue – and 0.4 eV/Å – dot-dashed, orange line

Table 3.11: Different adsorption structures of alkalis onto transition metal surfaces studied in the present work. The experimental results have been emphasised and are from Kiskinova, Pirug and Bonzel (1983) – $\Delta\phi$ – except for Na/Pt (111) from Bonzel, Pirug and Ritke (1991) – and Moré (1998) for Na/Pt (111) and K/Pt (111), van Hove (1994) for Na/Rh (111) and Gierer *et al* (1992) for K/Ru (0001). $\Delta\phi$ is the change in the work function from the clean in surface in electron volts, ΔE the energy difference for adsorption at the hcp site minus at the fcc site in milli electron volts, $z_{\mathrm{A-S}}$ the layer height of the adsorbate above its nearest-neighbour substrate atoms, $d_{\mathrm{A-S}}$ the corresponding distance, d_{12}, d_{23} and d_{bulk} are the average distances between first and second, second and third, and two layers in the bulk, correspondingly, b is the buckling in the first substrate layer and a the lateral relaxation in the first substrate layer. Positive values of b in the (2×2) cells denote that the unique atom is higher than the three symmetrically equivalent atoms of the top-most layer of the substrate

Unit cell	Site	$\Delta\phi$	ΔE	$z_{\mathrm{A-S}}$	$d_{\mathrm{A-S}}$	d_{12}	d_{23}	d_{bulk}	b	a
Na/Pt (111)										
$(\sqrt{3}\times\sqrt{3})$R30°	**hcp**	**−4.0**		**2.36**	**2.77**	**2.34**	**2.27**	**2.26**	**0**	
	hcp	−3.99	12	2.30	2.84	2.37	2.32	2.32	—	0.03
	fcc	−3.98		2.31	2.85	2.37	2.32	2.32	—	0.02
(2×2)	**hcp**	**−4.0**		**2.29**		**2.24-2.27**	**2.33**	**2.26**	**+0.09. . . +0.13**	
	hcp	−3.95	10	2.32	2.85	2.36	2.31	2.32	+0.08	0.02
	fcc	−3.96		2.31	2.85	2.36	2.31	2.32	+0.07	0.02
K/Pt (111)										
$(\sqrt{3}\times\sqrt{3})$R30°	**hcp**	**−4.1**		**2.71**	**3.15**	**2.29**	**2.25**	**2.26**	**0**	
	hcp	−3.62	11	2.69	3.16	2.36	2.31	2.32	—	0.02
	fcc	−3.52		2.70	3.17	2.36	2.31	2.32	—	0.02
(2×2)	**hcp**	**−4.4**		**2.70**	**3.12**	**2.28**	**2.26**	**2.26**	**0.07**	
	hcp	−4.07		2.68	3.15	2.36	2.31	2.32	0.03	0.02
Na/Rh (111)										
$(\sqrt{3}\times\sqrt{3})$R30°	**hcp**			**2.36**		**2.18**	**2.19**	**2.19**	**0**	**0.02**
	hcp	−3.39	20	2.38	2.89	2.19		2.25	—	0.05
	fcc	−3.38		2.40	2.90	2.20		2.25	—	0.04
K/Ru (0001)										
$(\sqrt{3}\times\sqrt{3})$R30°	**hcp**	**−3.8**		**2.94**	**3.33**	**2.10**	**2.14**	**2.14**	**0**	
	hcp	−3.12		2.93	3.36	2.15		2.19	—	0.04
Cs/Ru (0001)										
$(\sqrt{3}\times\sqrt{3})$R30°	**hcp**	**−3.9**		**3.16**	**3.52**	**2.09**	**2.14**	**2.14**	**0**	
	hcp	−3.26	6	3.10	3.51	2.15		2.19	—	0.03
	fcc	−3.24		3.09	3.51	2.15		2.19	—	0.05
(2×2)	**ot**	**−4.1**								
	hcp	−3.50	−0	3.11	3.52	2.15		2.19	+0.01	0.04
	fcc	−3.47		3.11	3.52	2.15		2.32	+0.02	0.05
(3×3)		**−3.7**								
	hcp	−2.90		3.19	3.58	2.14		2.32	+0.00	0.03

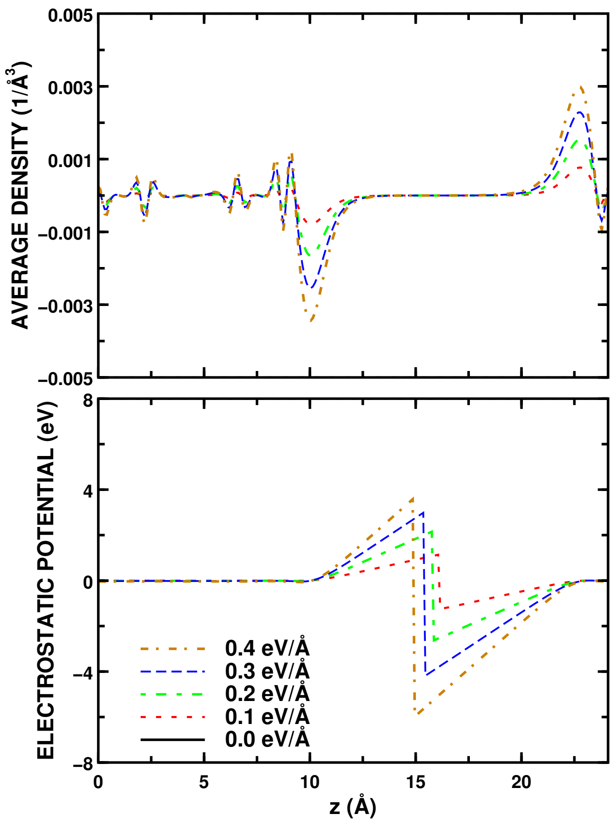

Figure 3.50: The change in the vertical density and electro-static potential averaged parallel to the surface in a Ru (0001) slab upon the application of a vertical electric field of 0.1 – red –, 0.2 – green –, 0.3 – blue – and 0.4 eV/Å – orange line

1700 – 1800 cm^{-1} to three- or four-fold hollow site; this follows the trend of a weakened internal bond at higher coordination site. This procedure of concluding the adsorption site based solely on the vibrational frequency has been criticised lately by Bradshaw and co-workers; please see *e. g.* the references cited by Davis *et al* (1997). The electronic effect upon adsorption is traditionally discussed in terms of the Blyholder model which is introduced in the Section 2.5.6. We will here also discuss the similarities between the adsorption of N_2 and CO; the molecules are iso-electronic but CO naturally carries a molecular dipole moment whereas N_2 not and the electronic states have higher symmetries in the latter molecule.

On Ru (0001) the adsorption was found to occur with the molecular axis parallel to the surface normal and with the carbon towards the surface in the electron stimulated desorption ion angle distributions – *ESDIAD* – by Madey (1979); the ultraviolet photoemission (Fuggle, Steinkilberg & Menzel, 1975) and electron energy loss spectroscopic (Thomas & Weinberg, 1978) results had already suggested this. The vibrational frequency for the internal C-O stretch mode was found from the high-resolution electron energy loss (Thomas & Weinberg, 1979; He, Dietrich & Jacobi, 1996) and infra-red adsorption spectra – *IRAS* – (Pfnür *et al*, 1980; Jakob, 1996) to be about 2000 cm^{-1}, thus close to the border-line between the on-top and bridge adsorption. However the on-top site was concluded first based on the vibrational frequency and the first structural determination with the low energy electron diffraction by Michalk *et al* (1983). In the low energy electron diffraction a clearly ordered pattern was observed at the coverage 1/3, showing the $(\sqrt{3} \times \sqrt{3})R30°$ order. The maximum coverage found using various methods is 0.68, thus close to 2/3. Already at low coverages the $(\sqrt{3} \times \sqrt{3})R30°$ pattern is detected, pointing to island formation with patches of the

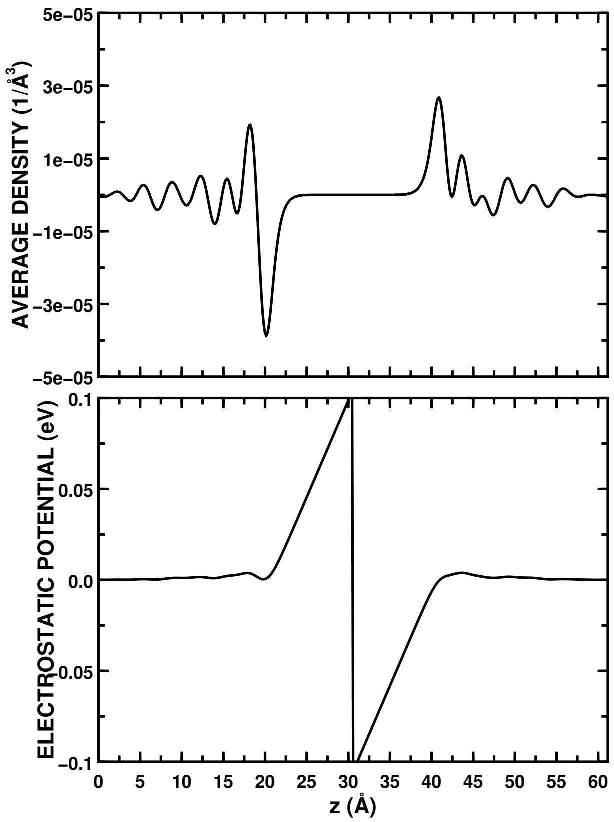

Figure 3.51: The change in the vertical density and electro-static potential averaged parallel to the surface in a jellium slab with the density corresponding to r_s=3 Bohr upon the application of a vertical electric field of 0.4 eV/Å

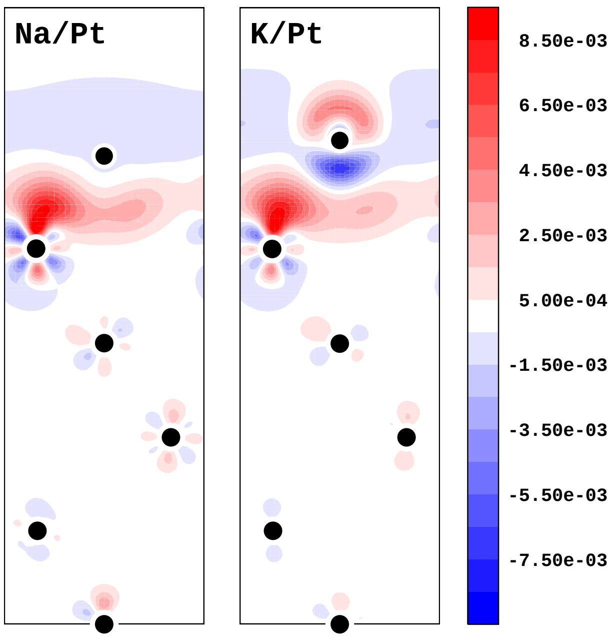

Figure 3.52: The change in the electron density upon the adsorption of the alkali atom sodium – left – and potassium – right – onto the Pt(111) surface in the $(\sqrt{3} \times \sqrt{3})$R30°-A$_{\mathrm{hcp}}$ structure, A = Na, K